





14 **Abstract**

15           Extreme climates affect the seasonal and interannual patterns of carbon (C) distribution  
16 due to the regimes of river inflow and thermal stratification within lentic ecosystems. Typhoons  
17 rapidly load substantial amounts of terrestrial C into subtropical small lakes, renewing and mixing  
18 the water column. We developed conceptual dissolved C models and hypothesized that  
19 allochthonous C loading and river inflow intrusion may affect the dissolved inorganic C (DIC)  
20 and dissolved organic C (DOC) distributions in a small subtropical lake under these extreme  
21 climates. A two-layer conceptual C models was developed to explore how the DIC and DOC  
22 fluxes respond to typhoon disturbances on seasonal and interannual time scales in a small  
23 subtropical lake (i.e., Yuan–Yang Lake) while simultaneously considering autochthonous  
24 processes such as algal photosynthesis, remineralization, and vertical transportation. Monthly  
25 field samplings were conducted to measure DIC, DOC, and chlorophyll *a* concentrations to  
26 compare the temporal patterns of fluxes between typhoon years (2015–2016) and non-typhoon  
27 years (2017–2018). The results demonstrated that net ecosystem production was 3.14 times higher  
28 in the typhoon years than in the non-typhoon years in Yuan–Yang Lake. The results suggested  
29 that the load of allochthonous C was the most crucial factor affecting the temporal variation of C  
30 fluxes in the typhoon years; on the other hand, the transportation rate shaped the seasonal C in the  
31 non-typhoon years due to thermal stratification within this small subtropical lake.

32



## 33 1. Introduction

34 The Intergovernmental Panel for Environmental Changes Sixth Assessment Report  
35 (IPCC AR6) (2021) suggested that, by 2050, not only is air temperature going to increase by at  
36 least about 1.5 °C but high-intensity storms and drought events will become more frequent as a  
37 result of global warming and climate change. In freshwater ecosystems, extreme climates may  
38 change the mixing regimes of water columns (Kraemer et al., 2021; Maberly et al., 2020;  
39 Woolway et al., 2020), heat wave events (Woolway et al., 2021a; Woolway et al., 2021b),  
40 droughts (Marcé et al., 2019), and floods (Woolway et al., 2018). Freshwater ecosystems store  
41 around 0.32 to 1.8 Pg C yr<sup>-1</sup>, which is approximately equivalent to shallow coastal areas; these  
42 ecosystems provide important services for human sustainability, such as acting as processing  
43 hotspots in regional C cycling (Aufdenkampe et al., 2011; Cole et al., 2007; Engel et al., 2018;  
44 Lauerwald et al., 2015; Raymond et al., 2013). Extreme weather events might induce stronger  
45 seasonal thermal stratification from spring to summer and longer overturn from autumn to  
46 winter, thereby changing the C distribution and transportation within water bodies (Kraemer et  
47 al., 2021; Olsson et al., 2022a; Woolway et al., 2020). The responses of C fluxes in small lakes  
48 (lake area < 1 km<sup>2</sup>) are sensitive to climate change due to the ease with which these C mix with  
49 water columns (Doubek et al., 2021; MacIntyre et al., 2021; Winslow et al., 2015). Moreover,  
50 storms induce dramatic changes in thermal stratification and water inflows (Lin et al., 2022;  
51 Olsson et al., 2022b; Vachon and Del Giorgio, 2014; Woolway et al., 2018). River inflows and  
52 wind turbulence mix the allochthonous C from sediments into the water column after storm  
53 events in small stratified lakes (Bartosiewicz et al., 2015; Czikowsky et al., 2018; Vachon and  
54 Del Giorgio, 2014). However, small lakes account for 25% to 35% of the total area of the earth's  
55 surface lakes (Cole et al., 2007; Downing et al., 2006; Raymond et al., 2013). However,  
56 compared to the case in larger lakes, C fluxes in small lakes remain uncertain because small  
57 lakes have usually been ignored in calculations of C flux on a global scale (Cole et al., 2007;  
58 Raymond et al., 2013). Thus, elucidation of the C fluxes in small lakes in extreme climates  
59 would be key to optimizing the estimations of global C fluxes in extreme climates.

60 Understanding the influences of physical, hydrological, and biogeochemical processes  
61 on the fates of C fluxes in smaller lake ecosystems is challenging work (Aufdenkampe et al.,  
62 2011; Cole et al., 2007; Raymond et al., 2013; Tranvik et al., 2009; Vachon et al., 2021;  
63 Woolway et al., 2018). This is not only because of difficulties in measurement but also because  
64 of the dynamics and interactions between factors and processes associated with C fluxes.  
65 Dissolved inorganic carbon (DIC) concentration is an important factor in estimating CO<sub>2</sub> fluxes  
66 within lake ecosystems (Smith, 1985). Among C fluxes in a freshwater body, the practical  
67 pressure of CO<sub>2</sub> (pCO<sub>2</sub>), defined as CO<sub>2</sub> emission across the air–water interface, is affected by  
68 DIC, water temperature, wind speed, and pH (Jähne et al., 1987; Smith, 1985). River inflows,



69 sediment, and respiration contribute to DIC loading into lakes (Hope et al., 2004; Vachon et al.,  
70 2021); simultaneously, autotrophic organisms, such as planktons and submerged vegetation,  
71 capture DIC via photosynthesis (Amaral et al., 2022; Nakayama et al., 2020; Nakayama et al.,  
72 2022). Moreover, calcification and mineralization may consume dissolved oxygen within water,  
73 inducing uncertainty in  $p\text{CO}_2$  estimation (Hanson et al., 2015; Lin et al., 2022; Nakayama et al.,  
74 2022). Dissolved organic carbon (DOC) might contribute to  $\text{CO}_2$  emission from lake water to  
75 the atmosphere through mineralization and remineralization within lake ecosystems (Hanson et  
76 al., 2015; Sobek et al., 2005). In subtropical freshwater ecosystems, DOC concentration is one  
77 of the vital factors in describing variances in mineralization and remineralization rates for  
78 dissolved C (Lin et al., 2022; Shih et al., 2019). Kossin et al. (2013) investigated global storm  
79 events with an accumulated rainfall of about 50 mm, which is approximately 10% to 40% of  
80 precipitation in a subtropical typhoon event. Other studies found that typhoon disturbances  
81 quickly mix, renew, or dilute the water in small subtropical lakes (Ejarque et al., 2021; Kimura  
82 et al., 2012; Kimura et al., 2017; Lin et al., 2022). Therefore, investigation of the magnitudes of  
83 DIC and DOC during typhoon disturbances is essential to understand the seasonal regimes and  
84 to estimate C fluxes in small subtropical lakes.

85 Typhoons' effects on C fluxes were studied in a small, two-layer stratified, subtropical  
86 lake, Yuan–Yang Lake (YYL) (Chiu et al., 2020; Jones et al., 2009; Lin et al., 2021; Lin et al.,  
87 2022). Jones et al. (2009) used the conceptual hydrology model and sensor data to estimate  $\text{CO}_2$   
88 emission in YYL during the typhoon disturbances that occurred in October 2004: 2.2 to 2.7 g C  
89  $\text{m}^{-2} \text{d}^{-1}$  of  $\text{CO}_2$  was released into the atmosphere.  $\text{CO}_2$  emissions into the atmosphere were  
90 recorded at around 3.0 to 3.7 g C  $\text{m}^{-2} \text{d}^{-1}$  because of substantial loads of terrestrial C via river  
91 inflows after strong typhoons in YYL (Chiu et al., 2020). Especially, vertical mixing, thermal  
92 stratification, and river retention regimes were essential physical processes in the C fluxes in  
93 YYL (Lin et al., 2021; Lin et al., 2022). These studies suggested that river intrusion and thermal  
94 stratification are key factors shaping the seasonal and interannual patterns of C fluxes during  
95 typhoon disturbances. River intrusion not only controlled the C fluxes, algal biomass, and  
96 nutrient loading, but also influenced the length of stratification and hydraulic retention times  
97 (Lin et al., 2021; Lin et al., 2022; Maranger et al., 2018; Nakayama et al., 2020; Olsson et al.,  
98 2022a; Olsson et al., 2022b; Zwart et al., 2017; Vachon and Del Giorgio, 2014). We  
99 hypothesized that allochthonous C loading and river inflow intrusion may affect the DIC and  
100 DOC distributions (**Figure 1**). At the same time, autochthonous processes in small subtropical  
101 lakes, such as algal photosynthesis, remineralization, and vertical transportation, must also be  
102 considered (**Figure 1**). Here, we followed our hypothesis to develop two-layer conceptual C  
103 models to assess C flux responses to typhoon disturbances in small subtropical lakes.

104



## 105 **2. Materials and methods**

### 106 **2.1 Study site**

107 YYL is a shallow (mean water depth: 4.3 m) and oligotrophic (total phosphorous: 10-  
108 20  $\mu\text{g-P L}^{-1}$ ; total nitrogen: 20-60  $\mu\text{g-N L}^{-1}$ ) subtropical mountain lake (Chou et al., 2000; Tsai et  
109 al., 2008; Wu et al., 2001) on Chi-Lan Mountain at around 1,640 asl in north-central Taiwan  
110 (24.58° N, 121.40° E) (**Figure 2**). Its water is brown because of its humic acid content (colored  
111 dissolved organic matter: 20-50 ppb QSE; mean pH: 5.4). YYL is surrounded by old-growth trees  
112 such as *Chamaecyparis formosensis*, *Chamaecyparis obtusa* var. *formosana*, and *Rhododendron*  
113 *formosanum* Heiml (Chou et al., 2000). The annual precipitation is over 3,000 mm yr<sup>-1</sup>, and  
114 typhoon precipitation contributes up to half of the total precipitation in YYL (Chang et al., 2007;  
115 Lai et al., 2006). Due to rapid renewal of the water body, the water retention time (or residence  
116 time) was around 4.4 days in typhoon Megi from 27 September to 1 October 2016 (Lin et al.,  
117 2022). The water surface temperature ranges from 15 to 25 °C during March to August, and the  
118 water column overturns in September (Kimura et al., 2012; Kimura et al., 2017; Lin et al., 2021).  
119 The concentrations of dissolved C (Lin et al., 2021), nutrients (Chiu et al., 2020; Tsai et al., 2008)  
120 and organisms (Shade et al., 2011) increase within YYL from autumn to winter. YYL is registered  
121 as a long-term ecological study site by the Ministry of Science and Technology (MOST) of Taiwan  
122 since 1992 and became part of the Global Lake Ecological Observatory Network (GLEON) in  
123 2004.

124

### 125 **2.2 Water sampling and chemical analysis**

126 We collected water quality samples (DOC, DIC, Chl. *a*) at water depths of 0.04, 0.50,  
127 1.00, 2.00, and 3.50 m at a buoy site (**Figure 2**). We also measured the water surfaces of six river  
128 inflows and an outflow monthly using a horizontal van Dorn bottle (2.20 L, acrylic) from January  
129 2015 to December 2018 (**Figure 2**). These samples were collected by using a portable hand pump  
130 and glass microfiber filter papers (47 mm GF/F, nominal pore size 0.70  $\mu\text{m}$ ; Whatman, Maidstone,  
131 Kent, UK) to obtain filtrate samples. Water samples were stored at around 4°C in a refrigerator  
132 until analysis. Samples were analyzed by using an infrared gas detector to detect DIC and DOC  
133 concentrations with persulfate digestion (model 1088 Rotary TOC autosampler; OI Analytical,  
134 College Station, TX, USA). The filter papers were kept in opaque bottles at around -25 °C in a  
135 refrigerator until the samples were analyzed by using a portable fluorometer (model 10-AU-005-  
136 CE; Turner Designs, Sunnyvale, CA, USA). In the laboratory, the filter papers were extracted  
137 with methanol to obtain the Chl. *a* concentration. These samples were analyzed for less than 72 h  
138 to prevent light and chemical degradation.

139

### 140 **2.3 Data analysis and numerical modeling**



141 Three water quality variables (DIC, DOC, and Chl. *a*) were compared between different  
142 layers (upper and lower layers), years (typhoon years and non-typhoon years), and seasons (spring,  
143 summer, autumn, and winter). First, we separated our investigation data into typhoon years and  
144 non-typhoon years as described in Sect. 2.3.1. Next, we developed a conceptual equations model  
145 to generate continuous DIC and DOC data at the upper and lower layers as shown in **Figure 1**.  
146 This helped us understand the transportation, photosynthesis, and remineralization rates between  
147 seasons and between typhoon and non-typhoon years (Sect. 2.3.2).

148

### 149 **2.3.1 Typhoon and non-typhoon years**

150 We collected meteorological data from a meteorological tower located about 1.0 km  
151 from YYL (Lin et al., 2021; Lin et al., 2022). Rainfall (model N-68; Nippon Electric Instrument,  
152 Tokyo, Japan) and wind speed (model 03001, R.M. Young, Traverse City, MI, USA) data were  
153 stored in a datalogger (model CR1000; Campbell Scientific, Logan, UT, USA) for every 10 min.  
154 River discharge ( $Q_{in}$ ,  $\text{m}^3 \text{d}^{-1}$ ) was estimated using the rainfall data and a water depth meter (model  
155 HOBO U20; Onset Computer, Bourne, MA, USA) at the end of a river inflow (**Figure 2**) for  
156 every 10 min by following the Manning formula. Transparency was estimated by using Secchi  
157 disc data measured at local times (GMT+08:00) from 10:00 to 14:00.

158 As **Table 1** shows, four strong typhoons were recorded, contributing a total of 2,254  
159 mm of precipitation in all 24 months of 2015 and 2016, accounting for 35.6% of annual  
160 precipitation. However, there no typhoon rainfall was recorded at YYL in 2017 and 2018; the total  
161 precipitation in that 2-year period was around 2,537 mm. There was no significant difference in  
162 average water depth between 2017 and 2018 (**Table 1**). The averaged discharge was less than 774  
163  $\text{m}^3 \text{d}^{-1}$  in 2017 and 2018. Thus, we considered 2015 and 2016 as typhoon years, and 2017 and  
164 2018 as non-typhoon years.

165

### 166 **2.3.2 Conceptual two-layer DIC and DOC model**

167 Nakayama et al. (2010) successfully developed a conceptual two-layer dissolved oxygen  
168 model based on the strong wind turbulence at Tokyo Bay. Additionally, Lin et al. (2021) pointed  
169 out that thermal stratification that inhibits vertical C flux between the upper and lower layers in  
170 shallow stratified lakes make it possible to develop conceptual two-layer C models (Lin et al.,  
171 2022; Nakayama et al., 2022), and the phytoplankton and remineralization effects on DIC and  
172 DOC fluxes ( $d\text{DIC}/dt$  and  $d\text{DOC}/dt$ ,  $\text{mg-C L}^{-1} \text{d}^{-1}$ ) were considered in a two-layer conceptual  
173 equation model as shown from **Equation 1** to **Equation 4**. The fluxes in the upper layer (from  
174 the water surface to 2.5 m water depth) were calculated as follows:



$$V_U \frac{dDIC_U}{dt} = Q_U DIC_R - Q_{out} DIC_U - V_U \alpha_{PU} Chl_U + V_U \alpha_{MU} DOC_U + A_I w_I (DIC_L - DIC_U) \quad (1)$$

$$+ Q_L DIC_L - \frac{A_S F_{CO2}}{C_U} + P a_U$$

$$V_U \frac{dDOC_U}{dt} = Q_U DOC_R - Q_{out} DOC_U - V_U \alpha_{MU} DOC_U + A_I w_I (DOC_L - DOC_U) \quad (2)$$

$$+ Q_L DOC_L + P b_U$$

175 Those in the lower layer (from 2.5 to 4.0 m water depth) are calculated as follows:

$$V_L \frac{dDIC_L}{dt} = Q_L DIC_R - V_L \alpha_{PL} Chl_L + V_L \alpha_{ML} DOC_L + A_I w_I (DIC_U - DIC_L) - Q_L DIC_L \quad (3)$$

$$+ \frac{A_B B F_{DIC}}{C_U} + P a_L$$

$$V_L \frac{dDOC_L}{dt} = Q_L DOC_R - V_L \alpha_{ML} DOC_L + A_I w_I (DOC_U - DOC_L) - Q_L DOC_L + P b_L \quad (4)$$

$$V_{total} = V_U + V_L \quad (5)$$

$$Q_{in} = Q_U + Q_L \quad (6)$$

176 where, total lake volume ( $V_{total}$ , 53,544 m<sup>3</sup>) departs to the upper layer ( $V_U$ , 45,456 m<sup>3</sup>) and to  
 177 the lower layer ( $V_L$ , 8,808 m<sup>3</sup>) (**Equation 5**), and where lake surface area ( $A_S$ ) is 36,000 m<sup>2</sup> and  
 178 the bottom of lake area ( $A_B$ ) is 3,520 m<sup>2</sup>. The interface is 2.5 m vertically, and the interface area  
 179 ( $A_I$ ) is 7,264 m<sup>2</sup> in YYL. The  $C_U$  is a coefficient value (= 1,000) to establish a standard unit for  
 180  $F_{CO2}$  (mg-C m<sup>-2</sup> d<sup>-1</sup>), considering the air–water CO<sub>2</sub> exchange by Fick's law as follows:

$$F_{CO2} = k_{CO2} \cdot K_H (pCO2_{water} - pCO2_{air}) \quad (7)$$

181 where  $k_{CO2}$  is the gas transfer velocity from wind speed empirical equations (Cole and Caraco,  
 182 1998; Jähne et al., 1987; Smith, 1985; Wanninkhof, 1992).  $K_H$  is Henry's coefficient calculated  
 183 by water temperature empirical equations (Plummer and Busenberg, 1982).  $pCO2_{air}$  (µatm) is  
 184 the CO<sub>2</sub> partial pressure in the atmosphere by using air pressure data (Lin et al., 2021; Lin et al.,  
 185 2022), and the atmospheric CO<sub>2</sub> concentration is assumed to be 400 ppm.  $pCO2_{water}$  (µatm) is  
 186 the CO<sub>2</sub> partial pressure at the water surface around 0.04 m water depth from water quality data  
 187 (temperature, pH, DIC concentration at water surface), and an empirical equation (Cai and  
 188 Wang, 1998) as followed by Lin et al. (2021).  $F_{CO2}$  contributed approximately half of the net  
 189 ecosystem production (NEP) across the water surface to the atmosphere in YYL (Lin et al.,  
 190 2021). In addition, because sediment carbon may be an important flux into shallow subtropical



191 lakes, the sediment C flux ( $BF_{DIC}$ ,  $BF_{DOC}$ , mg-C L<sup>-1</sup>) in the lower layer should be considered  
192 (Lin et al., 2022).

193 We assumed the river discharge and outflow discharge ( $Q_{out}$ , m<sup>3</sup> d<sup>-1</sup>) are quasi-steady  
194 state ( $Q_{in} = Q_{out}$ ), dividing into upper discharge ( $Q_U$ , m<sup>3</sup> d<sup>-1</sup>) and lower discharge ( $Q_L$ , m<sup>3</sup> d<sup>-1</sup>)  
195 (**Equation 6**). Lin et al. (2021) showed that the buoyancy frequencies in YYL are  $0.011 \pm 0.004$   
196 s<sup>-1</sup>,  $0.013 \pm 0.004$  s<sup>-1</sup>,  $0.006 \pm 0.003$  s<sup>-1</sup>, and  $0.007 \pm 0.004$  s<sup>-1</sup> from spring to winter, respectively,  
197 inhibiting the vertical profile DIC mixed due to stratification. We estimated the percentages of  
198  $Q_U$  and  $Q_L$  based on the buoyancy frequency following Lin et al. (2020 and 2022).  $Q_U$  values  
199 were 75%, 80%, 45%, and 50% of  $Q_{in}$  for spring to winter, respectively, and  $Q_L$  values were  
200 25%, 20%, 55%, and 50% of  $Q_{in}$ . The physical and biogeochemical regimes under climate  
201 change remain uncertain, such as biological compositions, mixing regimes, morphometric  
202 characteristics, air-water energy fluxes (evaporation and transpiration), and so on (Woolway et  
203 al., 2020). To simulate extreme climate scenarios, we shifted the ratio of  $Q_{in}$  for each season  
204 and tested the river intrusion hypothesis (**Figure 1**). We established two extreme conditions,  
205 labeled *Level 1* and *Level 2*. *Level 2* is the more extreme condition:  $Q_U$  is 80% (spring), 85%  
206 (summer), 50% (autumn), and 50% (winter) of  $Q_{in}$ ;  $Q_L$  is 20% (spring), 15% (summer), 50%  
207 (autumn), and 50% (winter) of  $Q_{in}$ . *Level 1* is the condition between the present and the *Level 2*  
208 condition:  $Q_U$  is 77% (spring), 82% (summer), 47% (autumn), and 50% (winter) of  $Q_{in}$ ;  $Q_L$   
209 is 23% (spring), 18% (summer), 53% (autumn), 50% (winter) of  $Q_{in}$ .

210 The contributions of photosynthesis production depended on the chlorophyll *a*  
211 concentration ( $Chl_U$ ,  $Chl_L$ , mg L<sup>-1</sup>) and on the absorption coefficients in the upper layer ( $\alpha_{PU}$ , d<sup>-1</sup>)  
212 and lower layer ( $\alpha_{PL}$ , d<sup>-1</sup>). The coefficients of DOC remineralization rates in the upper layer  
213 ( $\alpha_{MU}$ , d<sup>-1</sup>) and lower layer ( $\alpha_{ML}$ , d<sup>-1</sup>) were considered in the conceptual models as well. The  $Pa_U$ ,  
214  $Pa_L$ ,  $Pb_U$ , and  $Pb_L$  are constants in the conceptual models. To obtain unknown values ( $\alpha_{PU}$ ,  
215  $\alpha_{MU}$ ,  $\alpha_{PL}$ ,  $\alpha_{ML}$ ,  $w_I$ ,  $BF_{DIC}$ ,  $BF_{DOC}$ ,  $Pa_U$ ,  $Pa_L$ ,  $Pb_U$ , and  $Pb_L$ ), we applied multiple  
216 regression analysis. Additionally, these unknown values were tested by trial and error to obtain  
217 the parameters of the *best-fit* condition (Nakayama et al., 2022), dividing the seasonal and  
218 nonseasonal serranoids to learn the seasonal differences. The same parameters of the *best-fit*  
219 condition were used to obtain the extreme conditions for *Level 1* and *Level 2*. We used the  
220 coefficient of determination ( $R^2$ ) and the Nash-Sutcliffe model efficiency coefficient (NSE)  
221 (Nash and Sutcliffe, 1970) to quantify the performance of the equation model with DIC and DOC  
222 sampling data (observation data) for each simulation.

223

### 224 2.3.3 NEP of DIC and DOC

225 The net ecosystem production was defined as the difference between primary  
226 production and ecological respiration due to photosynthesis and respiration via biota (Dodds



227 and Whiles, 2020). Because we assumed that the C fluxes were dependent on the river inflows  
 228 in YYL (**Figure 2**), we could estimate the NEP by end-member analysis using the C  
 229 concentration of the river inflow and outflow (Lin et al., 2021; Nakayama et al., 2020) by  
 230 following **Equation 8** to **Equation 11**. The upper layer NEP of DIC flux ( $\text{mg C d}^{-1}$ ) was  
 231 obtained from **Equation 1** as follows:

$$\begin{aligned}
 \text{Upper NEP}_{\text{DIC}} &= C_U \alpha_{PU} Chl_U - C_U \alpha_{MU} DOC_U - C_U \frac{A_I w_I (DIC_L - DIC_U)}{V_U} - C_U \frac{P a_U}{V_U} \\
 &= C_U \frac{Q_U DIC_R + Q_L DIC_L - Q_{out} DIC_U}{V_U} - \frac{A_S}{V_U} F_{CO2} \\
 &= C_U \frac{1}{t_{rU}} \left( \frac{Q_U}{Q_{in}} DIC_R + \frac{Q_L}{Q_{in}} DIC_L - DIC_U \right) - F_C \\
 t_{rU} &= \frac{V_U}{Q_{in}}
 \end{aligned} \tag{8}$$

232

233 The upper layer NEP of DOC flux ( $\text{mg C d}^{-1}$ ) can be estimated from **Equation 2**:

$$\begin{aligned}
 \text{Upper NEP}_{\text{DOC}} &= C_U \alpha_{MU} DOC_U - C_U \frac{A_I w_I (DOC_L - DOC_U)}{V_U} - C_U \frac{P b_U}{V_U} \\
 &= C_U \frac{Q_U DOC_R + Q_L DOC_L - Q_{out} DOC_U}{V_U} \\
 &= C_U \frac{1}{t_{rU}} \left( \frac{Q_U}{Q_{in}} DOC_R + \frac{Q_L}{Q_{in}} DOC_L - DOC_U \right)
 \end{aligned} \tag{9}$$

234



235 The lower layer NEP of DIC flux ( $\text{mg C d}^{-1}$ ) from **Equation 3**:

$$\begin{aligned} \text{Lower NEP}_{\text{DIC}} &= C_U \alpha_{\text{PL}} Ch_L - C_U \alpha_{\text{ML}} \text{DOC}_L - C_U \frac{A_I w_I (\text{DIC}_U - \text{DIC}_L)}{V_L} - \frac{A_B B F_{\text{DIC}}}{V_L} \\ &- C_U \frac{P a_L}{V_L} = C_U \frac{Q_L (\text{DIC}_R - \text{DIC}_L)}{V_L} = C_U \frac{1}{t_{rL}} \frac{Q_L}{Q_{in}} (\text{DIC}_R - \text{DIC}_L) \end{aligned} \quad (10)$$

$$t_{rL} = \frac{V_L}{Q_{in}}$$

236

237 The lower layer NEP of DOC flux ( $\text{mg C d}^{-1}$ ) from **Equation 4**:

$$\begin{aligned} \text{Lower NEP}_{\text{DOC}} &= C_U \alpha_{\text{ML}} \text{DOC}_L - C_U \frac{A_I w_I (\text{DOC}_U - \text{DOC}_L)}{V_L} - \frac{A_B B F_{\text{DOC}}}{V_L} - C_U \frac{P b_L}{V_L} \\ &= C_U \frac{Q_L (\text{DOC}_R - \text{DOC}_L)}{V_L} = C_U \frac{1}{t_{rL}} \frac{Q_L}{Q_{in}} (\text{DOC}_R - \text{DOC}_L) \end{aligned} \quad (11)$$

238

239 Thus, the total NEP of DIC and DOC are:

$$\text{NEP}_{\text{DIC}} = \frac{V_U \text{Upper NEP}_{\text{DIC}} + V_L \text{Lower NEP}_{\text{DIC}}}{V_{\text{total}}} \quad (12)$$

$$\text{NEP}_{\text{DOC}} = \frac{V_U \text{Upper NEP}_{\text{DOC}} + V_L \text{Lower NEP}_{\text{DOC}}}{V_{\text{total}}} \quad (13)$$

240

241 where,  $F_C$  is  $\frac{A_S}{V_U} F_{\text{CO}_2}$  and  $t_{rU}$ ,  $t_{rL}$  are residence times (d) in the upper and lower layers,

242 respectively. These parameters were used for the *best-fit* condition as shown in **Table 2**.

243



244 **3. Results**

245 **3.1 DIC, DOC, and Chl. *a* concentrations in typhoon and non-typhoon years**

246 Our results demonstrated that there were no significant differences in DIC, DOC, and  
247 Chl. *a* concentration between the layers in the typhoon years 2015 and 2016; on the other hand,  
248 all these parameters differed significantly between the layers in the typhoon years 2017 and 2018  
249 (**Figure 3**). The average  $DIC_U$  was  $1.23 \text{ mg-C L}^{-1}$ , and  $DIC_L$  was  $3.66 \text{ mg-C L}^{-1}$ ; the  
250 average  $DOC_U$  was  $5.87 \text{ mg-C L}^{-1}$ , and  $DOC_L$  was  $8.02 \text{ mg-C L}^{-1}$ ; and the  $Chl_U$  and  $Chl_L$  were  
251  $18.5 \mu\text{g-C L}^{-1}$  and  $2.13 \mu\text{g-C L}^{-1}$ , respectively (**Figure 3**). However, t-test results showed no significant  
252 differences in DIC, DOC, and Chl. *a* concentrations ( $p$ -values  $\geq 0.05$  that no significant  
253 differences in DIC data among seasons in the typhoon years) (**Figure 4 a**). On the other hand, the  
254 DOC concentration showed significant differences between seasons in the typhoon years (**Figure**  
255 **4 c-d**). No significant differences between  $Chl_U$  and  $Chl_L$  were observed among the seasons  
256 (**Figure 4 e-f**). However, the standard deviations (SD) of DIC and DOC were higher in summer  
257 and autumn (**Figure 4**) due to terrestrial C loading (Chiu et al., 2020). In summer, the SD values  
258 of  $DIC_U$  and  $DOC_U$  were  $3.51 \text{ mg-C L}^{-1}$  and  $3.69 \text{ mg-C L}^{-1}$ , respectively (**Figure 4 a, c, e**). In  
259 autumn,  $DIC_L$  and  $DOC_L$  had the highest SD ( $4.06$  and  $4.17 \text{ mg-C L}^{-1}$ , respectively) (**Figure 4**  
260 **b, d**). Notably, the maximums of  $DIC_U$  and  $DOC_U$  were  $7.06$  and  $15.6 \text{ mg-C L}^{-1}$  and those of  
261  $DIC_L$  and  $DOC_L$  were  $10.9$  and  $19.8 \text{ mg-C L}^{-1}$ , respectively, in the typhoon years (**Figure 4 a-**  
262 **d**).

263 Positive Pearson correlations of  $0.45$  to  $0.80$  were observed between the DOC and DIC  
264 in the typhoon years (**Figure 5 a**). In the non-typhoon years, the upper layer  $DIC_L$  was the only  
265 variable negatively correlated with DOC in the upper and lower layers (**Figure 5 b**). The lower  
266 layer DIC was positively correlated with the  $Chl_L$  due to the abundant respiration in the lower  
267 layer (**Figure 5**).

268



269 **3.2 Performance of conceptual two-layer DIC and DOC models**

270 The results for the typhoon years demonstrated that the most of the seasonal scenarios  
271 were better fitting than the nonseasonal scenarios (**Figure 6**). Under the seasonal scenarios, the  
272  $DIC_U$  was around 1.5 to 5.0 mg-C L<sup>-1</sup> (**Figure 6 a-b**) and  $DIC_L$  was around 5.0 mg-C L<sup>-1</sup> stably  
273 (**Figure 6 d**). However, the NSE of  $DIC_L$  was 0.73 under the nonseasonal scenarios, which was  
274 higher than seasonal scenarios (NSE = 0.71) (**Table 2**), because  $DIC_L$  was elevated dramatically,  
275 by 40 mg-C L<sup>-1</sup>, under the nonseasonal scenarios during the 2016 typhoon period (**Figure 6 c**). In  
276 the non-typhoon years (2017-2018), the *best-fit* values of  $DIC_U$  and  $DIC_L$  did not differ  
277 significantly between the seasonal and nonseasonal scenarios ( $R^2$  and NSE were around 0.40 and  
278 0.70, respectively). These results demonstrated that  $DIC_U$  and  $DIC_L$  in the typhoon years must  
279 use the seasonal scenarios, whereas in the non-typhoon years they should use the nonseasonal  
280 scenarios. On the other hand, the DOC under the seasonal scenarios fit our observation data  
281 perfectly ( $R^2 = 0.91, 0.46$  and NSE = 0.95, 0.73 for  $DOC_U, DOC_L$ , respectively) (**Figure 6 e-h**,  
282 **Table 2**). Thus, the results suggested that the  $DOC_U$  and  $DOC_L$  must use the seasonal scenarios  
283 in both the typhoon and non-typhoon years.

284 As shown in **Table 2**, the parameters for the conceptual two-layer DIC and DOC models  
285 showed different regimes between the typhoon and non-typhoon years. In the typhoon years, the  
286 photosynthesis absorption rates ( $\alpha_{PU}, \alpha_{PL}$ ) were negative (photosynthesis < respiration) for each  
287 season. YYL was a C source due to a large allochthonous C loading during typhoons; the  
288 respiration was elevated by around 30- to 150-fold from summer to autumn. On the other hand,  
289 the transportation rates ( $w_I, w_{IL}$ ) were higher in autumn than in the other seasons (**Table 2**) due  
290 to weak stratification and large C loading during typhoons. Additionally, the higher  
291 remineralization rates during typhoon disturbances from summer to autumn resulted in positive  
292  $\alpha_{MU}$  and  $\alpha_{ML}$ . In the non-typhoon years, the remineralization rates were negative (**Table 2**).  
293 Thus, the results suggested that the conceptual two-layer C models may be reasonably to fit the  
294 observation data.

295



296 **3.3 Interannual and seasonal NEP in YYL**

297 The typhoon disturbances in summer and autumn played an important role in  
298 promoting the C released by YYL (**Table 3**). Overall, YYL released 245 mg-C d<sup>-1</sup> of DIC and  
299 415 mg-C d<sup>-1</sup> of DOC during the typhoon years; during the non-typhoon years, it released 51.7  
300 mg-C d<sup>-1</sup> of DIC and 22.8 mg-C d<sup>-1</sup> of DOC (**Table 3**). The average  $F_C$  was one to two times  
301 larger than NEP, and 219 and 133 mg-C d<sup>-1</sup> were released from YYL into the atmosphere in the  
302 typhoon and non-typhoon years, respectively (**Table 3**). In summer, the upper layer DIC and  
303 DOC consumed approximately 3.7 times more DIC in the typhoon years than in the non-  
304 typhoon years (**Table 3**). In autumn, 216 mg-C d<sup>-1</sup> of upper layer DIC was released; however,  
305 46.1 mg-C d<sup>-1</sup> of upper layer DOC was produced in the typhoon years. The upper layer  $NEP_{DIC}$   
306 was negative in autumn of the typhoon years, when 268 mg-C d<sup>-1</sup> more  $F_C$  was released  
307 compared to the non-typhoon years. In addition, the lower layer was most released of C into the  
308 outflow; however, the NEP in the lower layer was more than twice as high in summer than in  
309 autumn in the typhoon years (**Table 3**). The average of total  $NEP_{DIC}$  was 3.14 times more  
310 released C in the typhoon than in the non-typhoon years; The average of total  $NEP_{DOC}$  was  
311 increased 62.3 mg-C d<sup>-1</sup> of DOC between the typhoon years and non-typhoon years due to the  
312 over ten-times higher NEP in the upper layer (**Table 3**).

313 The ratios of DIC and DOC concentrations reveal the magnitudes of allochthonous  
314 DOC loading into YYL (Shih et al., 2019; Walvoord and Striegl, 2007), and the upper and lower  
315 layers show different patterns. In the typhoon years, the upper layer ratios decreased (higher  
316 DOC loading) from summer to autumn, whereas in the lower layer, DIC:DOC decreased from  
317 autumn to winter. In the non-typhoon years, the autumn DIC:DOC was the lowest, around 0.216  
318 to 0.351 (**Table 3**).

319



320 **3.4 Interannual responses of DIC and DOC to typhoons**

321 We simulated the responses of DIC and DOC flux to typhoons by using conceptual  
322 two-layer C models. The results showed that the DIC was more sensitive to typhoon  
323 disturbances than DOC under scenarios of *Level 1* and *Level 2* (**Figure 7-9**). Overall, the C level  
324 declined in the upper layers but increased in the lower layers (**Figure 7**). DIC and DOC in the  
325 upper layer tended to decline from 1.0 (*Level 1*) to 2.0 mg-C L<sup>-1</sup> (*Level 2*) (**Figure 7 a, c**); at the  
326 same time, they increased to 10.0 and 20.0 mg-C L<sup>-1</sup> in the lower layer under *Level 1* and *Level*  
327 *2*, respectively (**Figure 7 b, d**).

328 The DIC concentration in the upper layer was significantly lower in typhoon than non-  
329 typhoon years during spring and autumn under *Level 2* (**Figure 8 a-c**). Under the *best-fit* and  
330 *Level 1* conditions, DIC concentrations decreased significantly from winter to spring (**Figure 8**  
331 **c-d**). The lower layer DIC values under the *best-fit* and *Level 1* conditions differed significantly  
332 between the typhoon and non-typhoon years (**Figure 8 e-h**). The lower layer DIC under *Level 2*  
333 differed significantly from winter to spring only (**Figure 8 e, h**). On the other hand, upper layer  
334 DOC showed significant typhoon responses for each condition from winter to spring (**Figure 9**  
335 **a, d**). The upper layer DOC tended to differ more significantly under the extreme climates from  
336 summer to autumn (**Figure 9 b-c**). The lower layer DOC showed different typhoon responses  
337 between spring and the other seasons (**Figure 9 e-h**).  
338



#### 339 **4. Discussion**

340 Annual total precipitation was 40% higher in typhoon years than in non-typhoon years  
341 (**Table 1**). Water retention and typhoon-induced upwelling control the dynamics of DIC and  
342 DOC during summer and autumn (Chiu et al., 2020; Jones et al., 2009; Tsai et al., 2008; Tsai et  
343 al., 2011). Typhoon-induced upwelling affects water quality data differently between upper and  
344 lower layers (**Figure 3**). DIC, DOC, and Chl. *a* concentrations differ significantly between  
345 upper and lower layers in the typhoon years (**Figure 3**) due to thermal stratification (Chiu et al.,  
346 2020; Lin et al., 2022; Tsai et al., 2008; Tsai et al., 2011). In addition, the abundance of  
347 organisms leads to intensive respirations in the lower layers during the non-typhoon period; for  
348 example, an anoxic condition at the hypolimnion may affect C mineralization and  
349 remineralization rates in non-typhoon years (Carey et al., 2022; Chiu et al., 2020; Lin et al.,  
350 2022; Shade et al., 2010; Shade et al., 2011). Therefore, these physical and biogeochemical  
351 processes might describe different patterns between the upper and lower layers, as revealed by  
352 Pearson correlations (**Figure 5**).

353 Thermal stratification and allochthonous C loading may drive the responses of NEP to  
354 typhoons in YYL. In the typhoon years, the absolute values of NEP were higher than in the non-  
355 typhoon years (**Table 3**). We found that precipitation from typhoons loaded large amounts of  
356 allochthonous C into YYL during summer and autumn, which might describe the higher NEP in  
357 autumn compared to other seasons (**Table 3**). Typhoons dramatically changed the seasonal and  
358 interannual patterns of DIC fluxes due to river intrusion (**Figure 7 a-b; Figure 8**), which  
359 corresponds to our hypothesis (**Figure 1**) and to the results of previous studies (Chiu et al.,  
360 2020; Lin et al., 2021; Lin et al., 2022). In summer, the spatial differences in DIC and DOC  
361 between layers were inhibited due to strong thermal stratification, describing the positive upper  
362 NEP and lower negative NEP (Lin et al., 2021). The thermal stratification and anoxic condition  
363 may have been controlled by the seasonal and interannual patterns of DIC and DOC fluxes in  
364 the non-typhoon years (**Tables 2-3; Figure 6**). Additionally, because of the absence of typhoon-  
365 induced mixing and allochthonous C loading, the absolute values of total NEP in the non-  
366 typhoon years were less than those the non-typhoon years (**Table 3**). These results suggested  
367 that the allochthonous C loading was the most crucial factor for DIC and DOC fluxes in the  
368 typhoon years; on the other hand, the transportation rate shaped the seasonal C due to thermal  
369 stratification in the non-typhoon years.

370 With the conceptual two-layer C models (**Table 2**), photosynthesis absorption ( $\alpha_{PU}$ ,  
371  $\alpha_{PL}$ ), remineralization ( $\alpha_{MU}$ ,  $\alpha_{ML}$ ), and transportation ( $w_I$ ,  $w_{IL}$ ) well represented the seasonal  
372 variations of DIC and DOC data. These parameters of the conceptual two-layer C models  
373 appeared in reasonable patterns (**Table 2**). The higher remineralization and photosynthesis rates  
374 resulted in higher absolute values of NEP in the autumn of the typhoon years (**Tables 2-3**). In



375 the non-typhoon years, the photosynthesis rates contributed to the total NEP (**Tables 2-3**).  
376 Moreover, without the typhoon-induced mixing and refreshing of the water column, anoxic  
377 conditions may occur (Carey et al., 2022; Vachon et al., 2021), which could result in negative  
378 remineralization rates in non-typhoon years. Thus, the conceptual two-layer C models well  
379 characterizes the seasonal and interannual responses of DIC and DOC fluxes to typhoons in  
380 YYL.

381 Under extreme weather conditions, *Level 2* usually shifted to different typhoon  
382 responses for each season (**Figures 8-9**) due to extreme river intrusions. DIC changes more  
383 significantly than DOC under *Level 1* and *Level 2* (**Figures 7-9**), because the photosynthesis,  
384 transportation, and remineralization rates may crucially affect the seasonal and interannual  
385 patterns of DOC as well (**Figure 1**). Moreover, we compared the NEP with different model  
386 conditions as shown in **Figure 10**, demonstrating that the responses of  $NEP_{DIC}$  to typhoons  
387 differed dramatically between *Level 1* and *Level 2* (**Figure 10 a-c**); especially, the Upper  
388  $NEP_{DIC}$  released more C in the typhoon years and absorbed more C in the non-typhoon years  
389 than *Obs* (**Figure 10 a**). Not only were the absolute values of  $NEP_{DIC}$  over 3 times higher in the  
390 typhoon than the non-typhoon years (**Table 3**), but SD was higher in the typhoon years as well  
391 (**Figure 10**). However,  $NEP_{DOC}$  changed less under *Level 1* and *Level 2* (**Figure 10 d-f**), a  
392 finding that is consistent with our continuous DOC data (**Figure 7 c-d**). Processes such as  
393 respiration, mineralization, and sediment burial may impact DOC fluxes (Bartosiewicz et al.,  
394 2015; Hanson et al., 2015; Maranger et al., 2018). To our knowledge, bio-photochemical  
395 mineralization and degradation may play a key role in shaping C fluxes because colored DOC  
396 reduced ultraviolet radiation (UVR) and active photosynthetic radiation (PAR) (Alleson et al.,  
397 2021; Chiu et al., 2020; Schindler et al., 1996; Scully et al., 1996; Williamson et al., 1999).  
398 Thus, we suggest that photo-biochemical processes (such as the photo-mineralization) should be  
399 considered in the upper layer in order to clarify and validate the responses of the total C fluxes  
400 under extreme climates in a two-layer stratified lake.  
401



402 **5. Conclusions**

403 Our conceptual two-layer C model revealed that allochthonous and autochthonous  
404 processes both accounted for C flux responses to typhoon disturbances on seasonal and  
405 interannual scales by applying our proposed two-layer conceptual C model. Without typhoons,  
406 the strength of thermal stratification were the primary determinants the seasonal and interannual  
407 patterns of DIC and DOC concentrations data and NEP. Typhoon-induced upwelling and  
408 loading facilitated 102.2 mg-DIC d<sup>-1</sup> and 62.3 mg-DOC d<sup>-1</sup> in YYL, respectively (**Table 3**). We  
409 successfully developed two-layer conceptual C models to obtain continuous DIC and DOC data  
410 in YYL and to simulate extreme conditions. The changes in seasonal river intrusion regimes in  
411 YYL resulted in a 3-fold higher total NEP<sub>DIC</sub> in the typhoon years than in the non-typhoon  
412 years. However, our model should be improved under extreme climate scenarios by considering  
413 other autochthonous processes, such as sediment burial, photo-biochemical processes, and  
414 anoxic conditions. The present results suggest that physical processes (river intrusion and  
415 vertical transportation) and biogeochemical processes (mineralization, photosynthesis, and  
416 respiration) in a subtropical small lake accounted for the C flux responses to typhoons on  
417 seasonal and interannual time scales.  
418



419 **Competing interests**

420           The authors have no conflicts of interest to report.

421

422 **Acknowledgements**

423           The authors thank YS Hsueh, LC Jiang, and TY Chen for their help with water sample  
424 collection and chemistry analysis. This work was supported by the Japan Society for the  
425 Promotion of Science (JSPS) under grant nos. 22H05726, 22H01601, and 18KK0119 for K  
426 Nakayama; and by the Academia Sinica, Taiwan (AS-103-TP-B15), Ministry of Science and  
427 Technology, Taiwan (MOST 106-2621-M-239-001, MOST 107-2621-M-239-001, MOST 108-  
428 2621-M-239-001) for CY Chiu and JW Tsai. This study benefited from participation in the  
429 Global Lakes Ecological Observatory Network (GLEON).

430           Hao-Chi Lin: Conceptualization, Methodology, Investigation, Formal analysis,  
431 Writing – original draft. Keisuke Nakayama: Methodology, Supervision, Writing – review &  
432 editing, Conceptualization. Jeng-Wei Tsai: Investigation, Funding acquisition, Writing –review  
433 & editing. Chih-Yu Chiu: Funding acquisition, Writing – review & editing.

434



## 435 **References**

- 436 Allesson, L., Koehler, B., Thrane, J.-E., Andersen, T., and Hessen, D. O.: The role of  
437 photomineralization for CO<sub>2</sub> emissions in boreal lakes along a gradient of dissolved organic  
438 matter, *Limnol. Oceanogr.*, 66, 158–170, <https://doi.org/10.1002/lno.11594>, 2021.
- 439 Amaral, J. H. F., Melack, J. M., Barbosa, P. M., Borges, A. V., Kasper, D., Cortés, A. C., Zhou,  
440 W., MacIntyre, S., and Forsberg, B. R.: Inundation, Hydrodynamics and Vegetation  
441 Influence Carbon Dioxide Concentrations in Amazon Floodplain Lakes, *Ecosystems*, 25,  
442 911–930, <https://doi.org/10.1007/s10021-021-00692-y>, 2022.
- 443 Aufdenkampe, A. K., Mayorga, E., Raymond, P. A., Melack, J. M., Doney, S. C., Alin, S. R.,  
444 Aalto, R. E., and Yoo, K.: Riverine coupling of biogeochemical cycles between land,  
445 oceans, and atmosphere, *Front. Ecol. Environ.*, 9, 53–60, <https://doi.org/10.1890/100014>,  
446 2011.
- 447 Bartosiewicz, M., Laurion, I., and MacIntyre, S.: Greenhouse gas emission and storage in a  
448 small shallow lake, *Hydrobiologia*, 757, 101–115, [https://doi.org/10.1007/s10750-015-2240-](https://doi.org/10.1007/s10750-015-2240-2)  
449 2, 2015.
- 450 Cai, W.-J. and Wang, Y.: The chemistry, fluxes, and sources of carbon dioxide in the estuarine  
451 waters of the Satilla and Altamaha Rivers, Georgia, *Limnol. Oceanogr.*, 43, 657–668,  
452 <https://doi.org/10.4319/lo.1998.43.4.0657>, 1998.
- 453 Carey, C. C., Hanson, P. C., Thomas, R. Q., Gerling, A. B., Hounshell, A. G., Lewis, A. S. L.,  
454 Lofton, M. E., McClure, R. P., Wander, H. L., Woelmer, W. M., Niederlehner, B. R., and  
455 Schreiber, M. E.: Anoxia decreases the magnitude of the carbon, nitrogen, and phosphorus  
456 sink in freshwaters, *Glob. Change Biol.*, <https://doi.org/10.1111/gcb.16228>, 2022.
- 457 Chang, S.-C., Wang, C.-P., Feng, C.-M., Rees, R., Hell, U., and Matzner, E.: Soil fluxes of  
458 mineral elements and dissolved organic matter following manipulation of leaf litter input in  
459 a Taiwan *Chamaecyparis* forest, *For. Ecol. Manag.*, 242, 133–141,  
460 <https://doi.org/10.1016/j.foreco.2007.01.025>, 2007.
- 461 Chiu, C.-Y., Jones, J. R., Rusak, J. A., Lin, H.-C., Nakayama, K., Kratz, T. K., Liu, W.-C., Tang,  
462 S.-L., and Tsai, J.-W.: Terrestrial loads of dissolved organic matter drive inter-annual carbon  
463 flux in subtropical lakes during times of drought, *Sci. Total Environ.*, 717, 137052,  
464 <https://doi.org/10.1016/j.scitotenv.2020.137052>, 2020.
- 465 Chou, C.-H., Chen, T.-Y., Liao, C.-C., and Peng, C.-I.: Long-term ecological research in the  
466 Yuanyang Lake forest ecosystem I. Vegetation composition and analysis, *Bot. Bull. Acad.*  
467 *Sin.*, 41, 61–72, 2000.
- 468 Cole, J. J. and Caraco, N. F.: Atmospheric exchange of carbon dioxide in a low-wind  
469 oligotrophic lake measured by the addition of SF<sub>6</sub>, *Limnol. Oceanogr.*, 43, 647–656,  
470 <https://doi.org/10.4319/lo.1998.43.4.0647>, 1998.



- 471 Cole, J. J., Prairie, Y. T., Caraco, N. F., McDowell, W. H., Tranvik, L. J., Striegl, R. G., Duarte,  
472 C. M., Kortelainen, P., Downing, J. A., Middelburg, J. J., and Melack, J.: Plumbing the  
473 Global Carbon Cycle: Integrating Inland Waters into the Terrestrial Carbon Budget,  
474 *Ecosystems*, 10, 172–185, <https://doi.org/10.1007/s10021-006-9013-8>, 2007.
- 475 Czirkowsky, M. J., MacIntyre, S., Tedford, E. W., Vidal, J., and Miller, S. D.: Effects of Wind  
476 and Buoyancy on Carbon Dioxide Distribution and Air-Water Flux of a Stratified Temperate  
477 Lake, *J. Geophys. Res. Biogeosci.*, 123, 2305–2322, <https://doi.org/10.1029/2017JG004209>,  
478 2018.
- 479 Dodds, W. K. and Whiles, M. R.: *Freshwater Ecology: Concepts and Environmental*  
480 *Applications of Limnology*, Third Edition, Elsevier, United Kingdom, 748-762, 2020.
- 481 Doubek, J. P., Anneville, O., Dur, G., Lewandowska, A. M., Patil, V. P., Rusak, J. A., Salmaso,  
482 N., Seltmann, C. T., Straile, D., Urrutia-Cordero, P., Venail, P., Adrian, R., Alfonso, M. B.,  
483 DeGasperi, C. L., Eyto, E., Feuchtmayr, H., Gaiser, E. E., Girdner, S. F., Graham, J. L.,  
484 Grossart, H.-P., Hejzlar, J., Jacquet, S., Kirillin, G., Llames, M. E., Matsuzaki, S.-I. S.,  
485 Nodine, E. R., Piccolo, M. C., Pierson, D. C., Rimmer, A., Rudstam, L. G., Sadro, S., Swain,  
486 H. M., Thackeray, S. J., Thiery, W., Verburg, P., Zohary, T., and Stockwell, J. D.: The extent  
487 and variability of storm-induced temperature changes in lakes measured with long-term and  
488 high-frequency data, *Limnol. Oceanogr.*, 66, 1979–1992, <https://doi.org/10.1002/lno.11739>,  
489 2021.
- 490 Douville, H., Raghavan, K., Renwick, J., Allan, R. P., Arias, P. A., Barlow, M., Cerezo-Mota, R.,  
491 Cherchi, A., Gan, T. Y., Gergis, J., Jiang, D., Khan, A., Mba, W. P., Rosenfeld, D., Tierney,  
492 J., and Zolina, O.: *Water cycle changes*, Cambridge University Press, *Climate Change 2021:*  
493 *The Physical Science Basis. Contribution of Working Group I to 45 the Sixth Assessment*  
494 *Report of the Intergovernmental Panel on Climate Change*, 2021.
- 495 Downing, J. A., Prairie, Y. T., Cole, J. J., Duarte, C. M., Tranvik, L. J., Striegl, R. G.,  
496 McDowell, W. H., Kortelainen, P., Caraco, N. F., Melack, J. M., and Middelburg, J. J.: The  
497 global abundance and size distribution of lakes, ponds, and impoundments, *Limnol.*  
498 *Oceanogr.*, 51, 2388–2397, <https://doi.org/10.4319/lo.2006.51.5.2388>, 2006.
- 499 Ejarque, E., Scholz, K., Wohlfahrt, G., Battin, T. J., Kainz, M. J., and Schelker, J.: Hydrology  
500 controls the carbon mass balance of a mountain lake in the eastern European Alps, *Limnol.*  
501 *Oceanogr.*, 66, 2110–2125, <https://doi.org/10.1002/lno.11712>, 2021.
- 502 Engel, F., Farrell, K. J., McCullough, I. M., Scordo, F., Denfeld, B. A., Dugan, H. A., Eyto, E.  
503 de, Hanson, P. C., McClure, R. P., Nöges, P., Nöges, T., Ryder, E., Weathers, K. C., and  
504 Weyhenmeyer, G. A.: A lake classification concept for a more accurate global estimate of  
505 the dissolved inorganic carbon export from terrestrial ecosystems to inland waters, *Sci. Nat.*,  
506 105, 25, <https://doi.org/10.1007/s00114-018-1547-z>, 2018.



- 507 Hanson, P. C., Pace, M. L., Carpenter, S. R., Cole, J. J., and Stanley, E. H.: Integrating  
508 Landscape Carbon Cycling: Research Needs for Resolving Organic Carbon Budgets of  
509 Lakes, *Ecosystems*, 18, 363–375, <https://doi.org/10.1007/s10021-014-9826-9>, 2015.
- 510 Hope, D., Palmer, S. M., Billett, M. F., and Dawson, J. J. C.: Variations in dissolved CO<sub>2</sub> and  
511 CH<sub>4</sub> in a first-order stream and catchment: an investigation of soil-stream linkages, *Hydrol.*  
512 *Process.*, 18, 3255–3275, <https://doi.org/10.1002/hyp.5657>, 2004.
- 513 Jähne, B., Münnich, K. O., Börsinger, R., Dutzi, A., Huber, W., and Libner, P.: On the parameters  
514 influencing air-water gas exchange, *J. Geophys. Res. Oceans*, 92, 1937,  
515 <https://doi.org/10.1029/JC092iC02p01937>, 1987.
- 516 Jones, S. E., Kratz, T. K., Chiu, C.-Y., and McMahon, K. D.: Influence of typhoons on annual  
517 CO<sub>2</sub> flux from a subtropical, humic lake, *Glob. Change Biol.*, 15, 243–254,  
518 <https://doi.org/10.1111/j.1365-2486.2008.01723.x>, 2009.
- 519 Kimura, N., Liu, W.-C., Chiu, C.-Y., and Kratz, T.: The influences of typhoon-induced mixing in  
520 a shallow lake, *Lakes Reserv.: Res. Manag.*, 17, 171–183, <https://doi.org/10.1111/j.1440-1770.2012.00509.x>, 2012.
- 522 Kimura, N., Liu, W.-C., Tsai, J.-W., Chiu, C.-Y., Kratz, T. K., and Tai, A.: Contribution of  
523 extreme meteorological forcing to vertical mixing in a small, shallow subtropical lake, *J.*  
524 *Limnol.*, 76, 116–128, <https://doi.org/10.4081/jlimnol.2016.1477>, 2017.
- 525 Kossin, J. P., Olander, T. L., and Knapp, K. R.: Trend Analysis with a New Global Record of  
526 Tropical Cyclone Intensity, *J. Clim.*, 26, 9960–9976, <https://doi.org/10.1175/JCLI-D-13-00262.1>, 2013.
- 528 Kraemer, B. M., Pilla, R. M., Woolway, R. I., Anneville, O., Ban, S., Colom-Montero, W.,  
529 Devlin, S. P., Dokulil, M. T., Gaiser, E. E., Hambright, K. D., Hessen, D. O., Higgins, S. N.,  
530 Jöhnk, K. D., Keller, W., Knoll, L. B., Leavitt, P. R., Lepori, F., Luger, M. S., Maberly, S. C.,  
531 Müller-Navarra, D. C., Paterson, A. M., Pierson, D. C., Richardson, D. C., Rogora, M.,  
532 Rusak, J. A., Sadro, S., Salmaso, N., Schmid, M., Silow, E. A., Sommaruga, R., Stelzer, J. A.  
533 A., Straile, D., Thiery, W., Timofeyev, M. A., Verburg, P., Weyhenmeyer, G. A., and Adrian,  
534 R.: Climate change drives widespread shifts in lake thermal habitat, *Nat. Clim. Chang.*, 11,  
535 521–529, <https://doi.org/10.1038/s41558-021-01060-3>, 2021.
- 536 Lai, I.-L., Chang, S.-C., Lin, P.-H., Chou, C.-H., and Wu, J.-T.: Climatic Characteristics of the  
537 Subtropical Mountainous Cloud Forest at the Yuanyang Lake Long-Term Ecological  
538 Research Site, Taiwan, *Taiwania*, 51, 317–329, 2006.
- 539 Lauerwald, R., Laruelle, G. G., Hartmann, J., Ciais, P., and Regnier, P. A.: Spatial patterns in  
540 CO<sub>2</sub> evasion from the global river network, *Global Biogeochem. Cycles*, 29, 534–554,  
541 <https://doi.org/10.1002/2014GB004941>, 2015.
- 542 Lin, H.-C., Chiu, C.-Y., Tsai, J.-W., Liu, W.-C., Tada, K., and Nakayama, K.: Influence of



- 543 Thermal Stratification on Seasonal Net Ecosystem Production and Dissolved Inorganic  
544 Carbon in a Shallow Subtropical Lake, *J. Geophys. Res. Biogeosci.*, 126,  
545 <https://doi.org/10.1029/2020JG005907>, 2021.
- 546 Lin, H.-C., Tsai, J.-W., Tada, K., Matsumoto, H., Chiu, C.-Y., and Nakayama, K.: The impacts  
547 of the hydraulic retention effect and typhoon disturbance on the carbon flux in shallow  
548 subtropical mountain lakes, *Sci. Total Environ*, 803, 150044,  
549 <https://doi.org/10.1016/j.scitotenv.2021.150044>, 2022.
- 550 Maberly, S. C., O'Donnell, R. A., Woolway, R. I., Cutler, M. E. J., Gong, M., Jones, I. D.,  
551 Merchant, C. J., Miller, C. A., Politi, E., Scott, E. M., Thackeray, S. J., and Tyler, A. N.:  
552 Global lake thermal regions shift under climate change, *Nat Commun.*, 11, 1232,  
553 <https://doi.org/10.1038/s41467-020-15108-z>, 2020.
- 554 MacIntyre, S., Bastviken, D., Arneborg, L., Crowe, A. T., Karlsson, J., Andersson, A., Gålfalk,  
555 M., Rutgersson, A., Podgrajsek, E., and Melack, J. M.: Turbulence in a small boreal lake:  
556 Consequences for air-water gas exchange, *Limnol. Oceanogr.*, 66, 827–854,  
557 <https://doi.org/10.1002/lno.11645>, 2021.
- 558 Maranger, R., Jones, S. E., and Cotner, J. B.: Stoichiometry of carbon, nitrogen, and phosphorus  
559 through the freshwater pipe, *Limnol Oceanogr Lett*, 3, 89–101,  
560 <https://doi.org/10.1002/lo2.10080>, 2018.
- 561 Marcé, R., Obrador, B., Gómez-Gener, L., Catalán, N., Koschorreck, M., Arce, M. I., Singer, G.,  
562 and Schiller, D. von: Emissions from dry inland waters are a blind spot in the global carbon  
563 cycle, *Earth-Sci. Rev.*, 188, 240–248, <https://doi.org/10.1016/j.earscirev.2018.11.012>, 2019.
- 564 Nakayama, K., Kawahara, Y., Kurimoto, Y., Tada, K., Lin, H.-C., Hung, M.-C., Hsueh, M.-L.,  
565 and Tsai, J.-W.: Effects of oyster aquaculture on carbon capture and removal in a tropical  
566 mangrove lagoon in southwestern Taiwan, *Sci. Total Environ*, 156460,  
567 <https://doi.org/10.1016/j.scitotenv.2022.156460>, 2022.
- 568 Nakayama, K., Komai, K., Tada, K., Lin, H. C., Yajima, H., Yano, S., Hipsey, M. R., and Tsai, J.  
569 W.: Modeling dissolved inorganic carbon considering submerged aquatic vegetation, *Ecol.*  
570 *Model.*, 431, 109188, <https://doi.org/10.1016/j.ecolmodel.2020.109188>, 2020.
- 571 Nakayama, K., Sivapalan, M., Sato, C., and Furukawa, K.: Stochastic characterization of the  
572 onset of and recovery from hypoxia in Tokyo Bay, Japan: Derived distribution analysis  
573 based on “strong wind” events, *Water Resour. Res.*, 46,  
574 <https://doi.org/10.1029/2009WR008900>, 2010.
- 575 Nash, J. E. and Sutcliffe, J. V.: River flow forecasting through conceptual models, I A discussion  
576 of principles, *J. Hydrol.*, 10, 398–409, 1970.
- 577 Olsson, F., Mackay, E. B., Barker, P., Davies, S., Hall, R., Spears, B., Exley, G., Thackeray, S.  
578 J., and Jones, I. D.: Can reductions in water residence time be used to disrupt seasonal



- 579 stratification and control internal loading in a eutrophic monomictic lake?, *J. Environ.*  
580 *Manage.*, 304, 114169, <https://doi.org/10.1016/j.jenvman.2021.114169>, 2022a.
- 581 Olsson, F., Mackay, E. B., Moore, T., Barker, P., Davies, S., Hall, R., Spears, B., Wilkinson, J.,  
582 and Jones, I. D.: Annual water residence time effects on thermal structure: A potential lake  
583 restoration measure?, *J. Environ. Manage.*, 314, 115082,  
584 <https://doi.org/10.1016/j.jenvman.2022.115082>, 2022b.
- 585 Plummer, L. and Busenberg, E.: The solubilities of calcite, aragonite and vaterite in CO<sub>2</sub>-H<sub>2</sub>O  
586 solutions between 0 and 90°C, and an evaluation of the aqueous model for the system  
587 CaCO<sub>3</sub>-CO<sub>2</sub>-H<sub>2</sub>O, *Geochim. Cosmochim. Acta*, 46, 1011–1040,  
588 [https://doi.org/10.1016/0016-7037\(82\)90056-4](https://doi.org/10.1016/0016-7037(82)90056-4), 1982.
- 589 Raymond, P. A., Hartmann, J., Lauerwald, R., Sobek, S., McDonald, C., Hoover, M., Butman,  
590 D., Striegl, R., Mayorga, E., Humborg, C., Kortelainen, P., Dürr, H., Meybeck, M., Ciais, P.,  
591 and Guth, P.: Global carbon dioxide emissions from inland waters, *Nature*, 503, 355–359,  
592 <https://doi.org/10.1038/nature12760>, 2013.
- 593 Schindler, D. W., Curtis, P. J., Parker, B. R., and Stainton, M. P.: Consequences of climate  
594 warming and lake acidification for UV-B penetration in North American boreal lakes,  
595 *Nature*, 379, 705–708, <https://doi.org/10.1038/379705a0>, 1996.
- 596 Scully, N. M., McQueen, D. J., and Lean, D. R. S.: Hydrogen peroxide formation: The  
597 interaction of ultraviolet radiation and dissolved organic carbon in lake waters along a 43-  
598 75°N gradient, *Limnol. Oceanogr.*, 41, 540–548, <https://doi.org/10.4319/lo.1996.41.3.0540>,  
599 1996.
- 600 Shade, A., Chiu, C.-Y., and McMahon, K. D.: Seasonal and episodic lake mixing stimulate  
601 differential planktonic bacterial dynamics, *Microb. Ecol.*, 59, 546–554,  
602 <https://doi.org/10.1007/s00248-009-9589-6>, 2010.
- 603 Shade, A., Read, J. S., Welkie, D. G., Kratz, T. K., Wu, C. H., and McMahon, K. D.: Resistance,  
604 resilience and recovery: aquatic bacterial dynamics after water column disturbance, *Environ.*  
605 *Microbiol.*, 13, 2752–2767, <https://doi.org/10.1111/j.1462-2920.2011.02546.x>, 2011.
- 606 Shih, Y.-T., Chen, P.-H., Lee, L.-C., Liao, C.-S., Jien, S.-H., Shiah, F.-K., Lee, T.-Y., Hein, T.,  
607 Zehetner, F., Chang, C.-T., and Huang, J.-C.: Dynamic responses of DOC and DIC transport  
608 to different flow regimes in a subtropical small mountainous river, *Hydrol. Earth Syst. Sci.*,  
609 22, 6579–6590, <https://doi.org/10.5194/hess-22-6579-2018>, 2019.
- 610 Smith, S. V.: Physical, chemical and biological characteristics\* of CO<sub>2</sub> gas flux across the air-  
611 water interface, *Plant Cell Environ.*, 8, 387–398, <https://doi.org/10.1111/j.1365-3040.1985.tb01674.x>, 1985.
- 613 Sobek, S., Tranvik, L. J., and Cole, J. J.: Temperature independence of carbon dioxide  
614 supersaturation in global lakes, *Global Biogeochem. Cycles*, 19, GB2003,



- 615 <https://doi.org/10.1029/2004GB002264>, 2005.
- 616 Tranvik, L. J., Downing, J. A., Cotner, J. B., Loiselle, S. A., Striegl, R. G., Ballatore, T. J.,  
617 Dillon, P., Finlay, K., Fortino, K., Knoll, L. B., Kortelainen, P. L., Kutser, T., Larsen, S.,  
618 Laurion, I., Leech, D. M., McCallister, S. L., McKnight, D. M., Melack, J. M., Overholt, E.,  
619 Porter, J. A., Prairie, Y., Renwick, W. H., Roland, F., Sherman, B. S., Schindler, D. W.,  
620 Sobek, S., Tremblay, A., Vanni, M. J., Verschoor, A. M., Wachenfeldt, E. von, and  
621 Weyhenmeyer, G. A.: Lakes and reservoirs as regulators of carbon cycling and climate,  
622 *Limnol. Oceanogr.*, 54, 2298–2314, [https://doi.org/10.4319/lo.2009.54.6\\_part\\_2.2298](https://doi.org/10.4319/lo.2009.54.6_part_2.2298), 2009.
- 623 Tsai, J.-W., Kratz, T. K., Hanson, P. C., Kimura, N., Liu, W.-C., Lin, F.-P., Chou, H.-M., Wu, J.-  
624 T., and Chiu, C.-Y.: Metabolic changes and the resistance and resilience of a subtropical  
625 heterotrophic lake to typhoon disturbance, *Can. J. Fish. Aquat. Sci.*, 68, 768–780,  
626 <https://doi.org/10.1139/F2011-024>, 2011.
- 627 Tsai, J.-W., Kratz, T. K., Hanson, P. C., Wu, J.-T., Chang, W. Y. B., Arzberger, P. W., Lin, B.-S.,  
628 Lin, F.-P., Chou, H.-M., and Chiu, C.-Y.: Seasonal dynamics, typhoons and the regulation of  
629 lake metabolism in a subtropical humic lake, *Freshw. Biol.*, 53, 1929–1941,  
630 <https://doi.org/10.1111/j.1365-2427.2008.02017.x>, 2008.
- 631 Vachon, D. and Del Giorgio, P. A.: Whole-Lake CO<sub>2</sub> Dynamics in Response to Storm Events in  
632 Two Morphologically Different Lakes, *Ecosystems*, 17, 1338–1353,  
633 <https://doi.org/10.1007/s10021-014-9799-8>, 2014.
- 634 Vachon, D., Sponseller, R. A., and Karlsson, J.: Integrating carbon emission, accumulation and  
635 transport in inland waters to understand their role in the global carbon cycle, *Glob. Change*  
636 *Biol.*, 27, 719–727, <https://doi.org/10.1111/gcb.15448>, 2021.
- 637 Walvoord, M. A. and Striegl, R. G.: Increased groundwater to stream discharge from permafrost  
638 thawing in the Yukon River basin: Potential impacts on lateral export of carbon and  
639 nitrogen, *Geophys. Res. Lett.*, 34, <https://doi.org/10.1029/2007GL030216>, 2007.
- 640 Wanninkhof, R.: Relationship between wind speed and gas exchange over the ocean, J.  
641 *Geophys. Res. Oceans*, 97, 7373, <https://doi.org/10.1029/92JC00188>, 1992.
- 642 Williamson, C. E., Morris, D. P., Pace, M. L., and Olson, O. G.: Dissolved organic carbon and  
643 nutrients as regulators of lake ecosystems: Resurrection of a more integrated paradigm,  
644 *Limnol. Oceanogr.*, 44, 795–803, [https://doi.org/10.4319/lo.1999.44.3\\_part\\_2.0795](https://doi.org/10.4319/lo.1999.44.3_part_2.0795), 1999.
- 645 Winslow, L. A., Read, J. S., Hansen, G. J. A., and Hanson, P. C.: Small lakes show muted  
646 climate change signal in deepwater temperatures, *Geophys. Res. Lett.*, 42, 355–361,  
647 <https://doi.org/10.1002/2014GL062325>, 2015.
- 648 Woolway, R. I., Anderson, E. J., and Albergel, C.: Rapidly expanding lake heatwaves under  
649 climate change, *Environ. Res. Lett.*, 16, 94013, <https://doi.org/10.1088/1748-9326/ac1a3a>,  
650 2021a.



- 651 Woolway, R. I., Jennings, E., Shatwell, T., Golub, M., Pierson, D. C., and Maberly, S. C.: Lake  
652 heatwaves under climate change, *Nature*, 589, 402–407, [https://doi.org/10.1038/s41586-](https://doi.org/10.1038/s41586-020-03119-1)  
653 020-03119-1, 2021b.
- 654 Woolway, R. I., Kraemer, B. M., Lenters, J. D., Merchant, C. J., O'Reilly, C. M., and Sharma,  
655 S.: Global lake responses to climate change, *Nat. Rev. Earth Environ.*, 1, 388–403,  
656 <https://doi.org/10.1038/s43017-020-0067-5>, 2020.
- 657 Woolway, R. I., Simpson, J. H., Spiby, D., Feuchtmayr, H., Powell, B., and Maberly, S. C.:  
658 Physical and chemical impacts of a major storm on a temperate lake: a taste of things to  
659 come?, *Climatic Change*, 151, 333–347, <https://doi.org/10.1007/s10584-018-2302-3>, 2018.
- 660 Wu, J.-T., Chang, S.-C., Wang, Y.-S., and Hsu, M.-K.: Characteristics of the acidic environment  
661 of the Yuanyang Lake (Taiwan), *Bot. Bull. Acad. Sin.*, 42, 17–22, 2001.
- 662 Zwart, J. A., Sebestyen, S. D., Solomon, C. T., and Jones, S. E.: The Influence of Hydrologic  
663 Residence Time on Lake Carbon Cycling Dynamics Following Extreme Precipitation  
664 Events, *Ecosystems*, 20, 1000–1014, <https://doi.org/10.1007/s10021-016-0088-6>, 2017.  
665



666 **Table 1.** Comparison of rainfall and hydrological records between typhoon and non-typhoon  
667 years at Yuan–Yang Lake.

<b>Records</b>	<b>Typhoon years</b>	<b>Non-typhoon years</b>
Time period (year)	2015-2016	2017-2018
Total precipitation (mm)	6,332	3,795
Total typhoon rainfall (mm)	2,254	0
Average water depth (m ± SD)	4.54 ± 1.7	4.51 ± 1.5
Average river discharge (m <sup>3</sup> d <sup>-1</sup> )	3,717	2,943
Transparency (Secchi disc depth, m ± SD)	1.58 ± 0.45	1.38 ± 0.28

668



669 **Table 2.** Best-fit parameters of DIC and DOC two-layer conceptual model from 2015 to 2018.

	2015–2016 Typhoon years				2017–2018 Non-typhoon years				2015– 2016 Typhoon years	2017– 2018 Non- typhoon years
	Spring	Summer	Autumn	Winter	Spring	Summer	Autumn	Winter	Non- seasonal	Non- seasonal
<i>Upper layer</i>										
$F_{CO_2}$ (mg-C m <sup>2</sup> d <sup>-1</sup> )	291	245	422	127	231	143	104	175	276	163
$\alpha_{PU}$ (d <sup>-1</sup> )	-1.20	-33.1	-183.5	-29.1	8.0	6.0	30.0	7.77	-22.0	8.0
$\alpha_{MU}$ (d <sup>-1</sup> )	-0.0227	0.0203	0.08	-0.031	-0.01	-0.039	-0.033	-0.195	-0.035	-0.0238
$w_I$ (d <sup>-1</sup> )	0.230	0.172	1.38	0.30	0.10	0.0478	0.120	0.180	0.159	0.107
$Pa_U$ (d <sup>-1</sup> )	12560	-1317	-23750	9597	9880	14000	17600	10100	4457	12420
$Pb_U$ (d <sup>-1</sup> )	-21930	9461	-42130	-17070	-3630	-1251	-20820	-9289	-12760	-9119
$dDIC_U$ (R <sup>2</sup> , NSE)	0.305, 0.614								0.072,	0.403,
$dDOC_U$ (R <sup>2</sup> , NSE)	0.909, 0.953								0.299	0.650
									0.242,	0.320,
									0.569	0.918
<i>Lower layer</i>										
$\alpha_{PL}$ (d <sup>-1</sup> )	-0.627	-22.1	15.0	-0.878	1.49	-6.87	6.0	-16.6	-21.11	2.0
$\alpha_{ML}$ (d <sup>-1</sup> )	-0.025	0.123	0.0755	0.00973	-0.010	-0.0376	-0.04	-0.048	0.123	-0.019
$w_{IL}$ (d <sup>-1</sup> )	0.205	0.187	0.540	0.286	0.112	0.055	0.298	0.166	0.0868	0.176
$Pa_L$ (d <sup>-1</sup> )	100	-5662	-10500	-1013	151.6	2032	1216	909	-5662	-40.5
$Pb_L$ (d <sup>-1</sup> )	-6012	-7395	-53940	-9639	-1338	-6296	-19470	-8748	-12240	-9919
$BF_{DIC}$ , $BF_{DOC}$ (mg-C L <sup>-1</sup> )					0.04,					
					0.00					
$dDIC_L$ (R <sup>2</sup> , NSE)	0.452, 0.707								0.192,	0.440,
$dDOC_L$ (R <sup>2</sup> , NSE)	0.460, 0.728								0.306	0.731
									0.234,	0.128,
									0.338	0.525

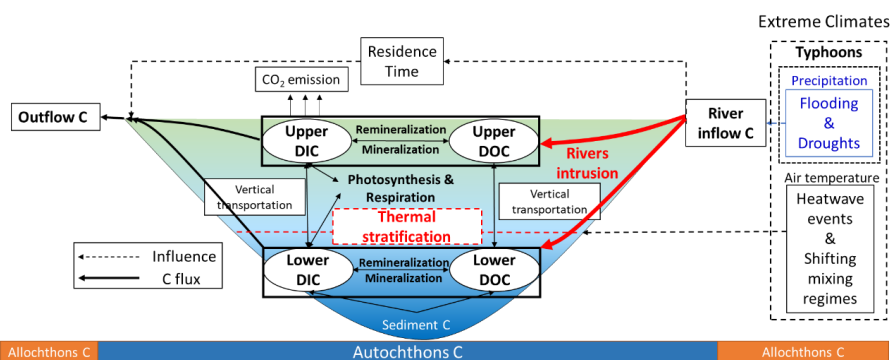


671 **Table 3.** Seasonal averages of C fluxes ( $\text{mg-C d}^{-1}$ ) for each season in YYL. Positive values are  
 672 shown in the C sink (*black*), and negative ones show the values after C was released (*red*).

		$F_C$	Flux ( $\text{mg C d}^{-1}$ )		$\frac{\text{DIC}_U}{\text{DOC}_U}$	$\frac{\text{DIC}_L}{\text{DOC}_L}$	Total ( $\text{mg C d}^{-1}$ )	
			Upper NEP	Lower NEP			NEP <sub>DIC</sub>	NEP <sub>DOC</sub>
<u><i>Typhoon</i></u> <u><i>years</i></u>		<b>Average: -219</b>	-	-	-	-	<b>-150</b>	<b>-9.69</b>
Spring	DIC	-231	-243	-45.2	0.658	0.568	-210	62.1
	DOC	-	70.8	17.2				
Summer	DIC	-194	29.1	-313	0.193	0.511	-26.4	18.8
	DOC	-	118	-495				
Autumn	DIC	-351	-216	-659	0.349	0.475	-288	-151
	DOC	-	46.1	-1167				
Winter	DIC	-100	-96.4	36.5	0.442	0.372	-74.8	31.2
	DOC	-	40.5	-16.9				
<u><i>Non-typhoon</i></u> <u><i>years</i></u>		<b>Average: -133</b>	-	-	-	-	<b>-47.8</b>	<b>52.6</b>
Spring	DIC	-129	-180	-94.9	0.524	0.634	-166	-7.06
	DOC	-	21.4	-67.1				
Summer	DIC	-183	5.80	-58.1	0.260	0.423	-4.57	73.8
	DOC	-	115	-140				
Autumn	DIC	-82.6	95.0	35.9	0.216	0.351	85.5	95.9
	DOC	-	168	-272				
Winter	DIC	-138	-128	6.04	0.449	0.436	-106	33.7
	DOC	-	34.0	32.1				

673

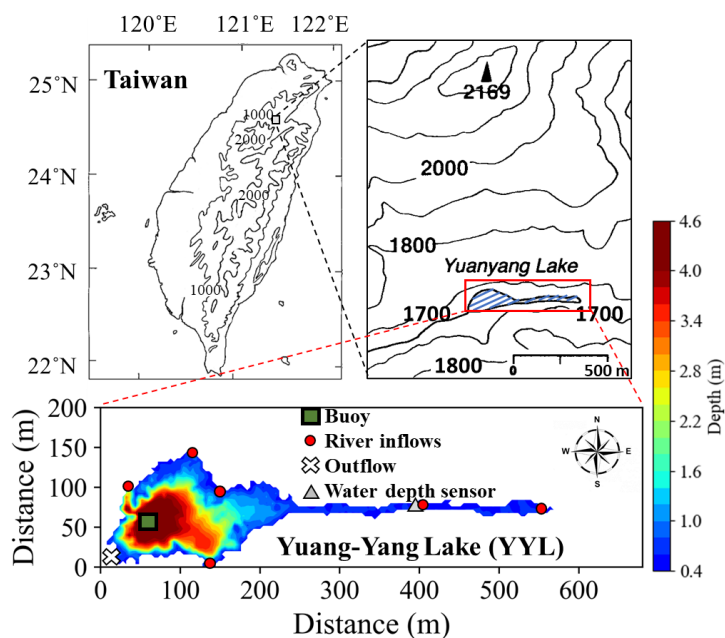
674



675

676 **Figure 1.** Conceptual diagram of river intrusion (*red arrows*) and thermal stratification  
677 (*red dashed line*) dominant responses of DIC and DOC in a subtropical two-layer  
678 stratified lake under extreme climates.

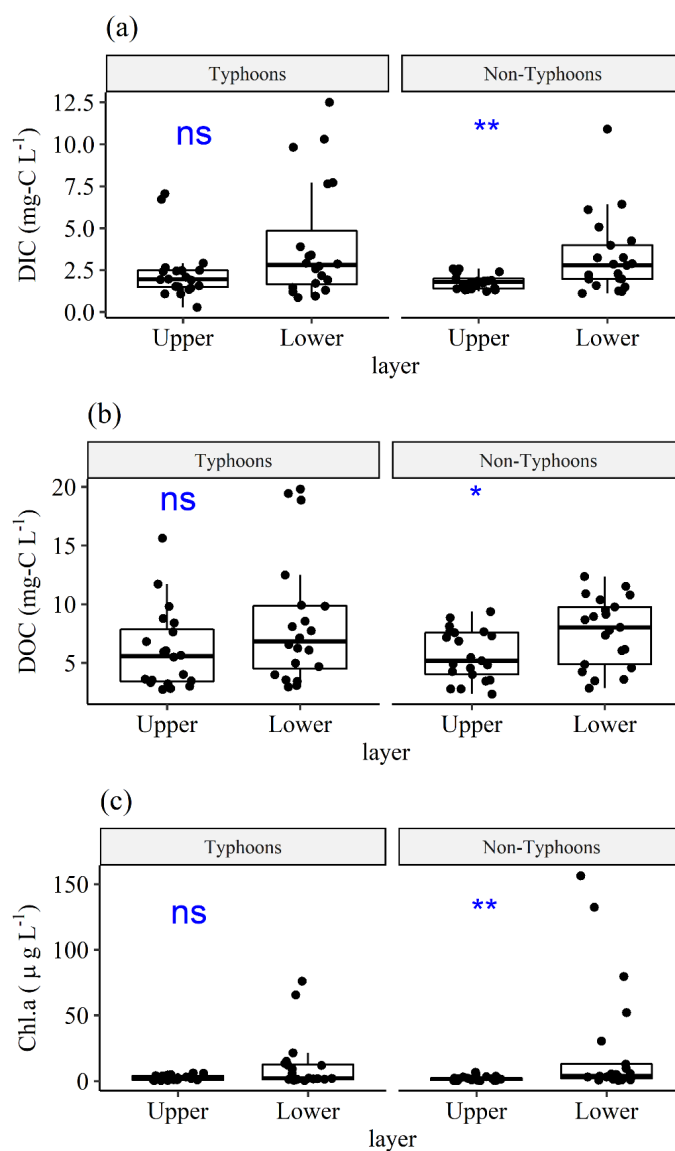
679



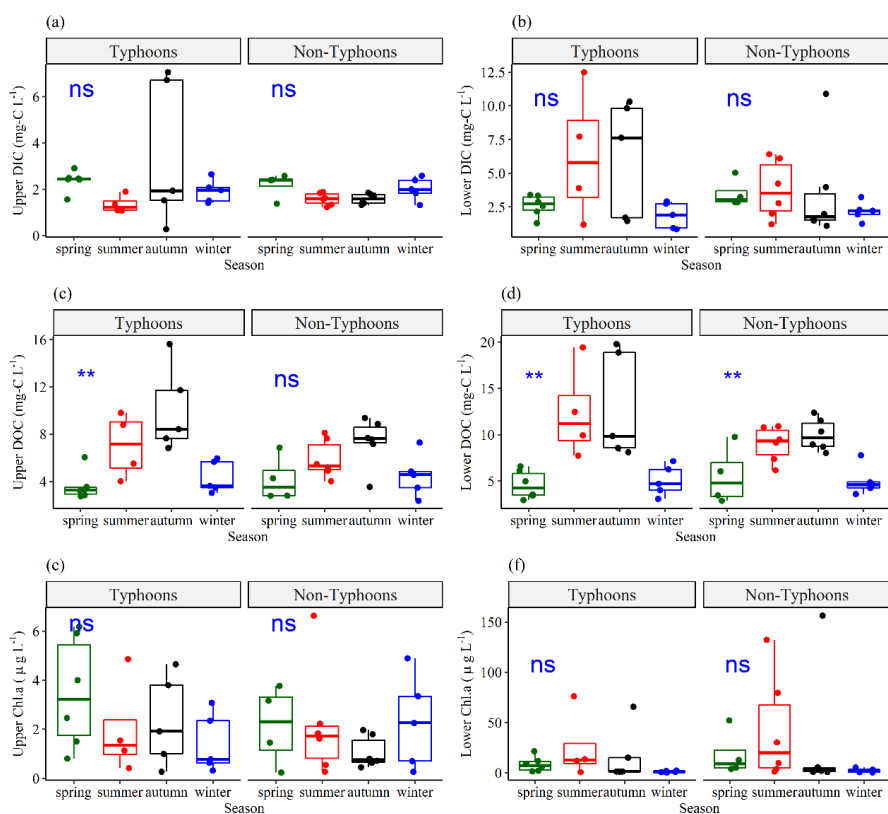
680

681 **Figure 2.** Sampling locations and bathymetry maps of Yuan–Yang Lake (YYL). The  
682 *dark green rectangle* shows the buoy station, which is at the deepest site of the lake. The  
683 *red points* and *white cross* show the river mouths of the inflows and outflow,  
684 respectively. The *gray triangle* shows the location of the water depth sensor.

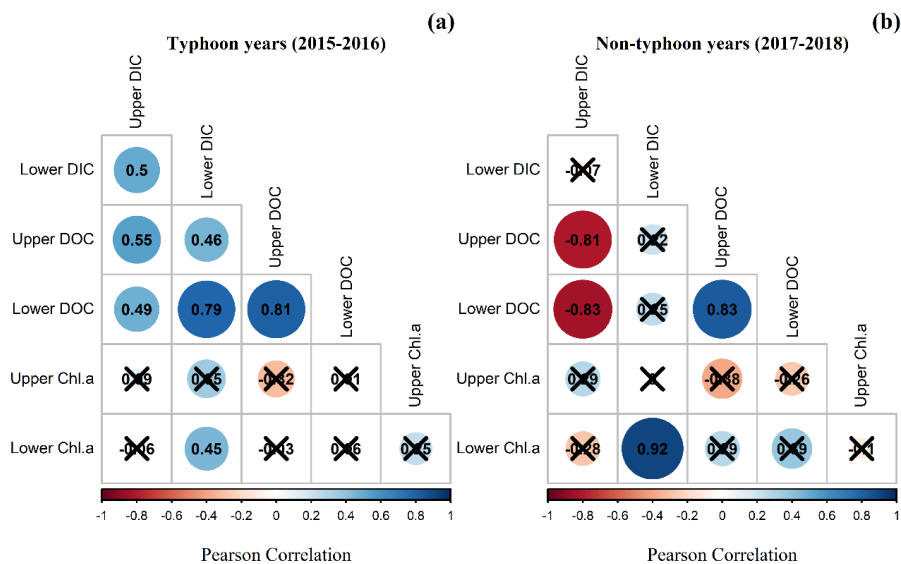
685



686  
687 **Figure 3.** Comparisons of (a) DIC, (b) DOC, and (c) Chl. *a* between upper ( $DIC_U$ ,  
688  $DOC_U$ ,  $Chl_U$ ) and lower ( $DIC_L$ ,  $DOC_L$ ,  $Chl_L$ ) layers, grouped by typhoon and non-  
689 typhoon years. The *bullet points* show the water sampling data. We used a t-test to  
690 obtain *p*-values. The **ns** show *p*-values  $\geq 0.05$ , \* show *p*-values from 0.05 to 0.01, and  
691 \*\* show *p*-values from 0.01 to 0.001 by t-test.



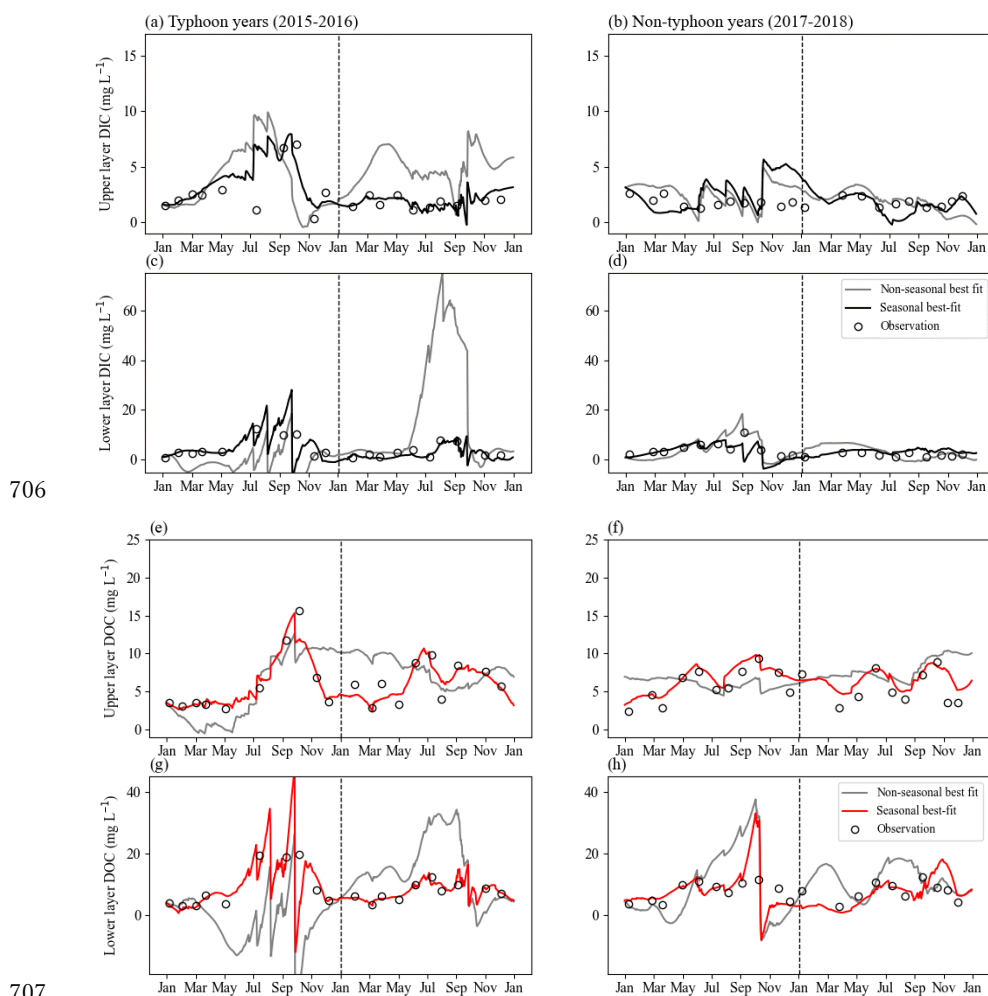
692  
 693 **Figure 4.** Seasonal variations of (a) upper layer DIC ( $DIC_U$ ), (b) lower layer DIC  
 694 ( $DIC_L$ ), (c) upper layer DOC ( $DOC_U$ ), (d) lower layer DOC ( $DOC_L$ ), (e) upper layer Chl.  
 695 *a* ( $Chl_U$ ), (f) lower layer Chl. *a* ( $Chl_L$ ) grouped by typhoon and non-typhoon years. The  
 696 *bullet points* show water sampling data. To know the seasonality, we used one-way  
 697 ANOVA to obtain the p-values. The **ns** show p-values  $\geq 0.05$ , \* show p-values from  
 698 0.05 to 0.01, and \*\* show p-values are from 0.01 to 0.001.  
 699



700

701 **Figure 5.** Pearson correlation coefficients of DIC, DOC, Chl. a concentration at upper  
 702 layer and lower layer DIC ( $DIC_U$ ,  $DIC_L$ ), DOC ( $DOC_U$ ,  $DOC_L$ ), Chl. a ( $Chl_U$ ,  $Chl_L$ )  
 703 during (a) typhoon years and (b) non-typhoon years. The *black-crosses* show  
 704 insignificant values ( $p$ -values are  $> 0.05$ ).

705



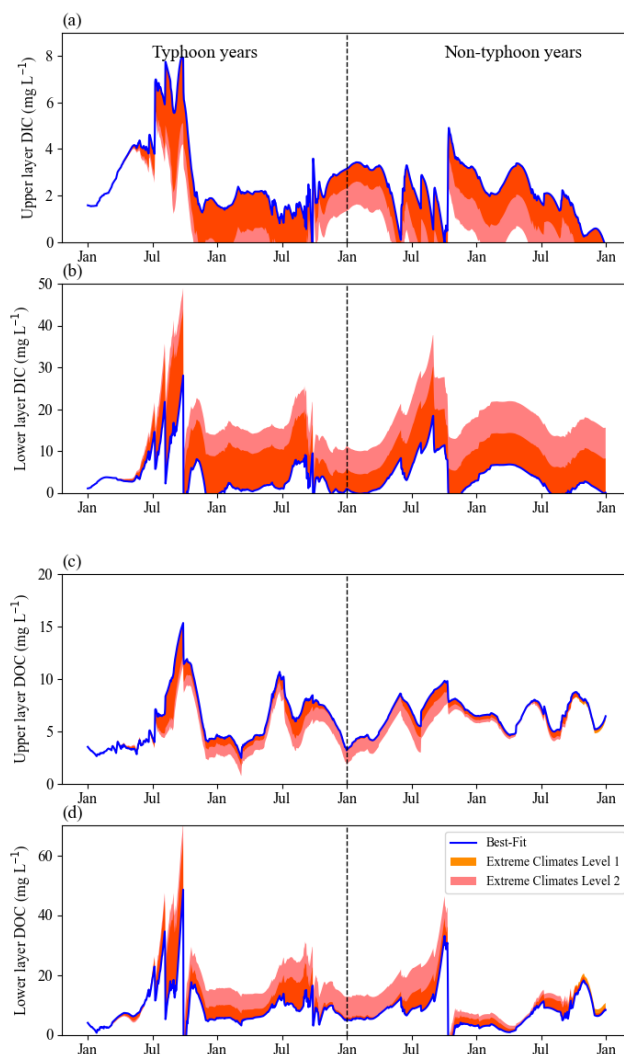
706

707

708 **Figure 6.** Continuous daily DIC and DOC data at (a, b, e, f) upper layer ( $DIC_U$ ,  $DOC_U$ )  
 709 and (c, d, g, h) lower layer ( $DIC_L$ ,  $DOC_L$ ) by using conceptual equations models. The  
 710 gray lines show the original data, the blue lines show the nonseasonal data, the black lines  
 711 show the best fit for DIC, the red lines show the best-fit for DOC (Table 2), and the empty  
 712 dots show water sampling (observation) data for each month.

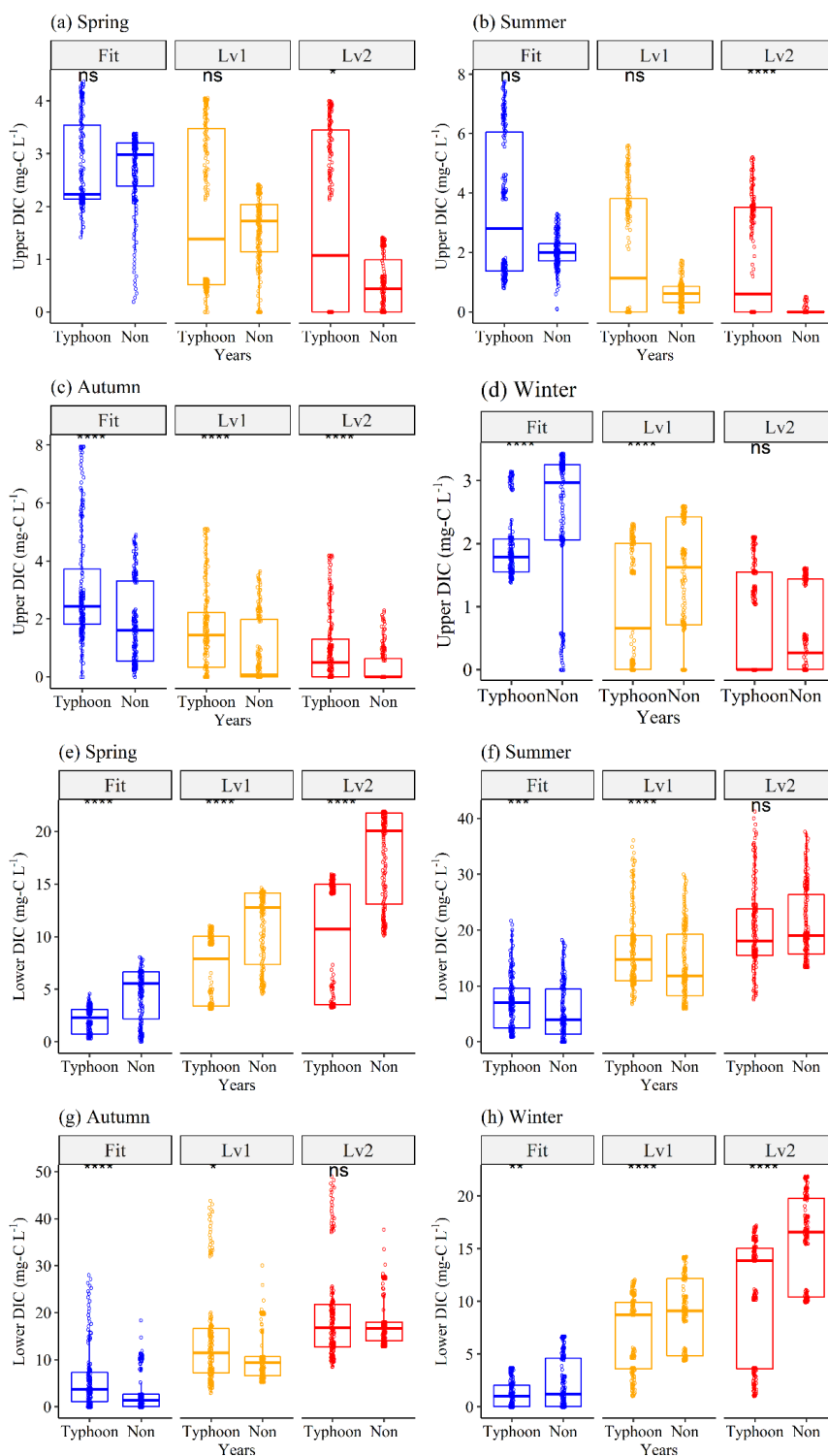


713



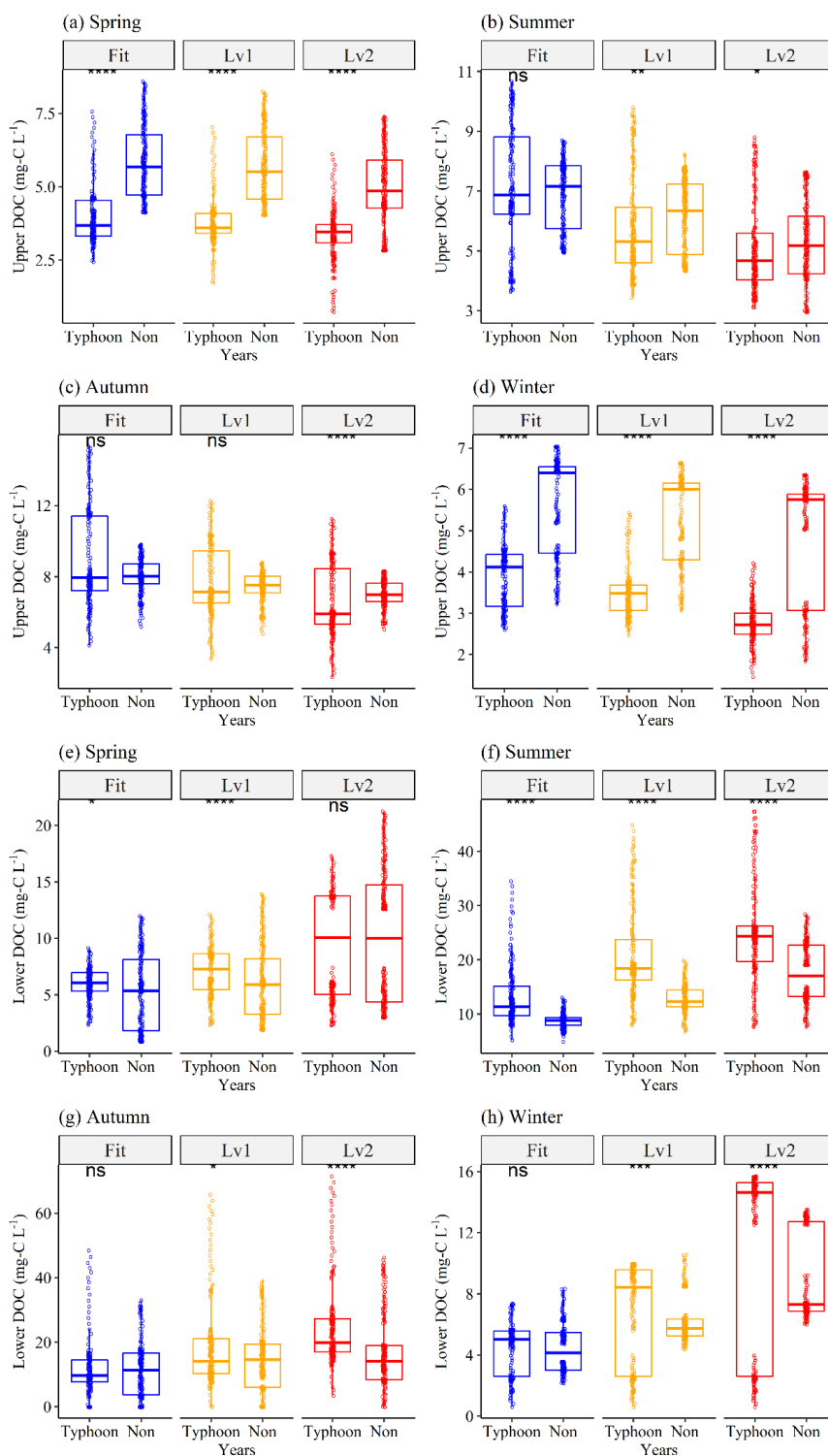
714

715 **Figure 7.** Continuous daily DIC and DOC data at (a, c) upper layer ( $DIC_U$ ,  $DOC_U$ ) and  
716 (b, d) lower layer ( $DIC_L$ ,  $DOC_L$ ) by using the conceptual equation model under extreme  
717 climates from 2015 to 2018. Blue lines are original best-fit data as in Figure 4, in which  
718 the parameters of the DIC model in non-typhoon years are under the nonseasonal  
719 scenario and the others are under the seasonal scenario as in Table 2. Orange regions  
720 show Level 1; pink regions show Level 2.



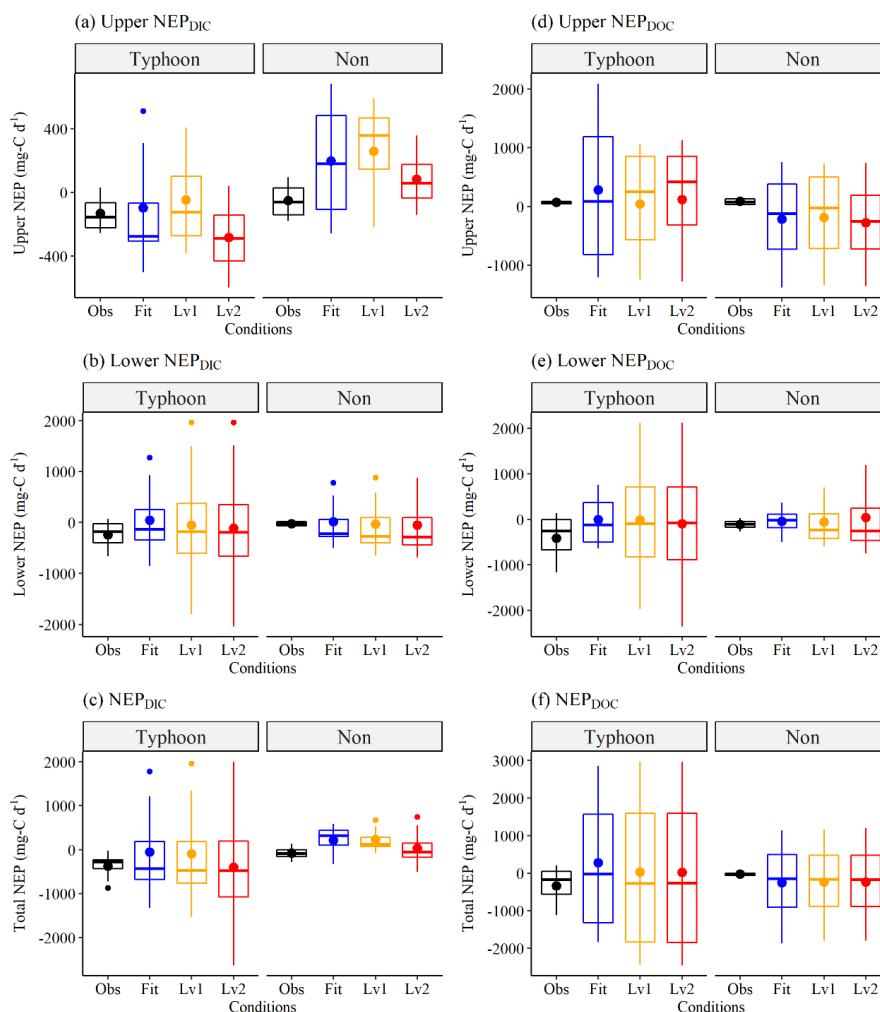


722 **Figure 8.** Seasonal responses of continuous **(a-d)** upper layer DIC and **(e-h)** lower layer  
723 DIC ( $\text{mg-C L}^{-1}$ ) between typhoon (*Typhoon*) and non-typhoon (*Non*) years for each  
724 season as in **Figure 8**. *Fit* (blue boxes) condition shows the best-fit data by using the  
725 conceptual two-layer C model; *Lv1* (yellow boxes) and *Lv2* (red boxes) show the extreme  
726 climates. The *empty dots* show the continuous DIC and DOC data. The **ns** show  $p$ -values  
727  $\geq 0.05$ , \* show  $p$ -values from 0.05 to 0.01, \*\* show  $p$ -values from 0.01 to 0.001; \*\*\*\*  
728 show  $p$ -values less than 0.0001 by using a t-test.





730 **Figure 9.** Seasonal responses of **(a-d)** upper layer DOC and **(e-h)** lower layer DOC (mg-  
731 C L<sup>-1</sup>) between typhoon (*Typhoon*) and non-typhoon (*Non*) years for each season as in  
732 **Figure 8.** *Fit (blue boxes)* condition shows the best-fit data by using the conceptual two-  
733 layer C model; *Lv1 (yellow boxes)* and *Lv2 (red boxes)* show the extreme climates. *Empty*  
734 *dots* show the continuous DIC and DOC data. The **ns** show *p*-values  $\geq 0.05$ , \* show *p*-  
735 values from 0.05 to 0.01, \*\* show *p*-values from 0.01 to 0.001; \*\*\*\* show *p*-values less  
736 than 0.0001 by using a t-test.



737

738 **Figure 10.** Interannual (a) Upper NEP<sub>DIC</sub>, (b) Lower NEP<sub>DIC</sub>, (c) NEP<sub>DIC</sub>, (d)  
 739 Upper NEP<sub>DOC</sub>, (e) Lower NEP<sub>DOC</sub>, and (f) NEP<sub>DOC</sub> flux (mg-C d<sup>-1</sup>) grouped by typhoon  
 740 and non-typhoon years. *Obs* condition (*black boxes*) show the observation data as in  
 741 **Figure 6**; *Fit* condition (*blue- boxes*) show the best-fit data by using the conceptual two-  
 742 layer C model as in **Figure 6**; *Level 1* (*yellow boxes*) and *Level 2* (*red boxes*) show the  
 743 extreme scenarios as in **Figure 7**.

744